3D printing geopolymers: A review

Hui Zhong, Mingzhong Zhang*

Department of Civil, Environmental and Geomatic Engineering, University College London, London, WC1E 6BT, UK

Abstract: Geopolymers have been considered as a promising alternative to cementitious materials for 3D printing to enhance sustainability of the construction industry. This paper presents a critical review of the state-of-the-art of 3D printing geopolymers from the perspectives of production process, printability requirement, mix design, early-age material properties and sustainability, with a special focus on the effects of different factors such as matrix composition, reinforcement type, curing regime and printing configuration on the fresh and hardened properties of 3D printed geopolymers. The relationship between key fresh properties and printability of geopolymers is discussed, based on which the potential optimal mix proportions are obtained, containing the blended precursors of fly ash, ground granulated blast-furnace slag and silica fume, liquid or solid activator, river sand with a maximum size of 2 mm, thixotropic additives (e.g., nano clay), and retarder (e.g., sucrose). This paper aims to summarise the recent advances in the development of 3D printing techniques suitable for geopolymers and geopolymers feasible for 3D printing, and to identify the knowledge gap, remaining challenges, and opportunities for future research.

Keywords: 3D concrete printing; Alkali-activated materials; Rheology; Mechanical properties; Sustainability; Durability

1. Introduction

The primary impetus of developing 3D printing technology, also known as additive manufacturing, in the realm of the construction industry is to increase the productivity of construction work [1]. Besides, it has a great potential to reduce construction wastes and enhance the shape freedom of constructed objects [2, 3]. It was reported that utilising 3D printing in construction can help reduce the fabrication waste, labour cost and production time by 30-60%, 50-80% and 50-70%, respectively [4]. Thus, 3D concrete printing has attracted a considerable number of interests worldwide in recent years while its evolving stage is slow compared to other industries.

Contour crafting developed in the mid-1990s is the first additive manufacturing technology in construction [5] based on the technology of fused deposition modelling [2, 6]. Later on, particle bed printing motivated by the technology of stereolithography [2, 7] came into view, which selectively deposits the binder liquid into the powder bed to bind the powder particles [1]. Hitherto, extrusion-based 3D printing is the most popular additive manufacturing method in the construction industry where the object is constructed via the layer-by-layer deposition of the material extruded from the

* Corresponding author. E-mail address: mingzhong.zhang@ucl.ac.uk (M. Zhang)

nozzle [1, 2, 8]. For most 3D printed concrete, Portland cement is the major binder material accounting for about 15-45% of the total mix proportion [9]. Besides, the binder content of 3D printed cementitious materials is typically higher than that of conventional mould-cast cementitious materials [10]. However, the increasing usage of Portland cement may result in higher material cost along with lower sustainability, given that the production of Portland cement contributes to around 8% of the global CO_2 emissions [11, 12]. Therefore, more studies have recently been focused on the feasibility of adopting a greener binder, geopolymer, to develop sustainable 3D printed concrete using either extrusion-based [13-15] or particle bed printing [16, 17] techniques.

Geopolymer, also known as alkali-activated material, is an inorganic polymer synthesised through the reaction between aluminosilicate materials and alkaline activators [18]. In summary, the current studies on 3D printing of geopolymers consider the effects of different factors including matrix composition, reinforcement, curing condition, test configuration and printing configuration on the fresh and hardened properties using a trial-and-error approach, as illustrated in Fig. 1. Up to now, the mix design and properties of 3D printed cementitious materials especially at early ages have been extensively reviewed [2, 5, 8, 9, 19, 20]. However, only a few studies [2, 9, 21] briefly discussed the mix design and properties of geopolymers for 3D printing. As the material behaviour of geopolymers, especially the rheology is significantly different from that of cementitious materials, and the rheological behaviour has a conspicuous influence on its printability. Thus, a critical review is urgently required to report the state-of-the-art of 3D printing geopolymers and identify some remaining challenges to address for their potential applications.

This paper aims to comprehensively review the mix design, printability, fresh and hardened properties of 3D printed geopolymers (3DPG) considering different factors shown in Fig. 1, as well as the economic and environmental benefits. It is worth mentioning that only the studies focusing on the extrusion-based 3DPG are reviewed here, while those [16, 17, 22, 23] concentrating on particle bed printing are not considered as the relevant research is very limited and most of the existing products produced by particle bed printing are not applicable for structural applications. Firstly, the procedure of extrusion-based 3D printing is briefly introduced in terms of four main steps including mixing, pumping, extruding, and building, which can highlight the difference between 3D printing of cementitious materials and 3D printing of geopolymers in terms of equipment and technique. Then, various parameters of characterising the printability of 3DPG along with the printability requirements are given. Afterwards, the fresh and hardened properties and sustainability of 3DPG are critically reviewed, with a special focus on the effects of matrix composition, reinforcement, curing condition, test configuration and printing configuration, and the relationship between critical fresh properties and printability for geopolymers. Lastly, the potential optimal mix proportions are summarised and discussed in depth.

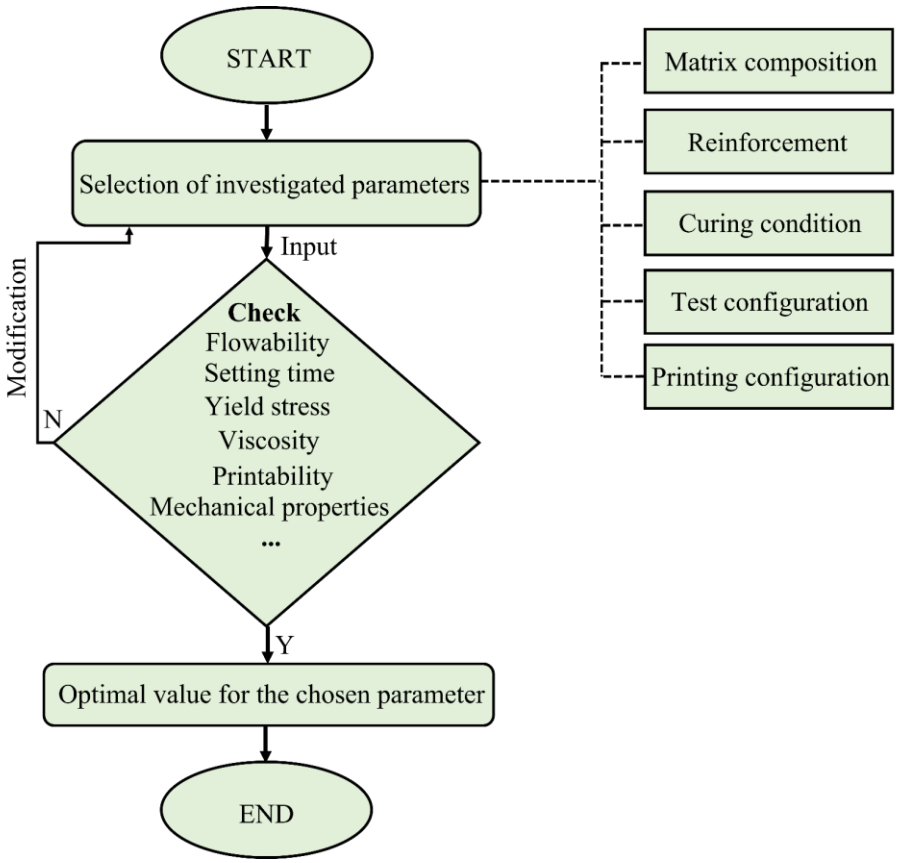

Fig. 1. Schematic diagram of the trial-and-error method used for 3D printed geopolymers (3DPG) (based on [9]).

2. 3D printing of geopolymers

2.1. General

At microscale, two main stages occur concurrently during the synthesis of geopolymer, i.e., dissolution and polycondensation [18, 24, 25]. When the alkaline activator is in contact with the aluminosilicate binder, the dissolution stage is initiated to break the surface bonds of the binder (e.g. $Si\text{-}O\text{-}Si$ and $Al\text{-}O\text{-}Al$ bonds in fly ash (FA)) dissolving the aluminate and silicate, which renders the formation of reactive ionic species [26-28]. The concentration of alkaline activator has a distinct effect on the dissolution degree [29]. The ionic species from the dissolution stage contain numerous groups of $Si\text{-}OH$ and $Al\text{-}OH$ that would condense during the polycondensation stage to form the 3D aluminosilicate gel [30, 31]. It should be pointed out that the above reactions are significantly influenced by the characteristics of binders [32, 33].

Table 1 summarises the available literature included in this paper in terms of raw materials, curing conditions and measured properties, indicating that the most commonly used binder type in 3DPG was a combination of low calcium FA, ground granulated blast-furnace slag (GGBS) and silica fume (SF) [13, 14, 34-42], while the other binder types such as limestone (LS) [43], metakaolin (MK) [44], steel slag (SS) [45], and calcium carbonate (CC) [46] were adopted together with FA or GGBS. Typically, the content of FA, GGBS and SF ranged from 60-95%, 1.67-30%, and 1.67-30% (by mass

of the total binder), respectively. The alkaline activator was utilised in either liquid or solid state, while the widely used type was a combination of NaOH and Na_2SiO_3 [14, 27, 34, 36, 38, 44-47]. The activator modulus (SiO_2/Na_2O (or K_2O)) employed by different studies ranged from 0.5 to 2.0. Similar to 3D printed cementitious materials, only fine aggregates with relatively small sizes (less than 2 mm) were employed for the development of 3DPG, while coarse aggregates are typically inhibited since they are difficult to pass through most of the existing hoses and nozzles in the 3D printing systems [48]. It should be noted that a limit is needed for the incorporated dosage of fine aggregates [34] and the aggregate-to-binder ratio (Agg/b) of most 3DPG mixtures ranged from 1.2 to 1.9. Different kinds of additives were applied to tailor the fresh and hardened properties of geopolymers, especially printability. For instance, the addition of attapulgite nano clay can help improve the yield stress of 3DPG, leading to better buildability [49]. Regarding the extrusion-based 3DPG, the use of conventional steel reinforcement is a challenge due to the extrusion and deposition processes [42]. Thus, randomly distributed short fibres including glass, steel, polypropylene (PP) and polyvinyl alcohol (PVA) fibres with different lengths and diameters were added during the mixing of 3DPG to enhance the ductility [39-41, 47, 50]. For instance, 3D printed strain-hardening geopolymer composites containing 2.0% PVA fibre were developed to mitigate the brittleness of plain 3DPG [51]. Apart from fibres, stainless steel cables with a diameter of 1000-2000 μm were utilised to improve the mechanical properties of 3DPG [39, 41, 42]. Different from the incorporation of fibres during the mixing, the above studies inserted the steel cables into the deposited geopolymers by a direct extruder feeding system, which may reduce the risk of printing failure caused by reduced printability. As illustrated in Table 1, most printed samples were cured under ambient temperature or standard curing condition (20 ± 1 °C and $95\% \pm 5\%$ relative humidity) until the ages for hardened properties testing. Elevated temperature curing was also used. For instance, Muthukrishnan et al. [50] applied microwave heating after printing to enhance the bond strength of 3DPG, as well as the mechanical properties and durability. The measured properties of 3DPG presented in existing studies mainly include flowability, setting time, yield stress, viscosity, structural build-up, thixotropy, printability, density, porosity, drying shrinkage, compressive strength, flexural strength, flexural ductility, tensile strength, and bond strength, which will be systemically discussed in Sections 3 and 4, considering different influencing factors.

Table 1 Summary of raw materials, curing conditions and measured properties collected from studies on extrusion-based 3D printed geopolymers (3DPG).

Ref.	Binder	Activator		L/b (or Act/b or W/s)	Additive	Aggregate		Fibre	Curing condition	Measured properties
		Type	SiO_2/Na_2O (or K_2O)			Type	Agg/b	Type (weight or volume)		
[13]	FA85%+GGBS5%+SF10%	KOH+K_2SiO_3	-	L/b (0.51)	Actigel+cellulose (thixotropic additive)	River sand	1.51	-	-	Evolution of thixotropy, density, compressive strength, flexural strength, tensile bond strength, microstructure
[45]	GGBS90%+SS10%	NaOH+Na_2SiO_3	0.5-1.0	W/s (0.33)	Deformer+superplasticiser+redispersible latex	-	-	-	-	Evolution of dynamic yield stress, plastic viscosity, evolution of specified rebuilding energy
[14]	FA100%, FA95%+GGBS5% or SF5%, FA90%+GGBS10% or SF10%, FA90%+GGBS5%+SF5%, FA96.7%+GGBS1.67%+SF1.67%, FA93.3%+GGBS3.3%+SF3.3%, FA91.7%+GGBS6.67%+SF1.67%, FA91.7%+GGBS1.67%+SF6.67%	NaOH+Na_2SiO_3	1.8	L/b (0.46)	-	River sand	1.5	-	Ambient temperature (25 ± 2 ºC)	Structural build-up behaviour[b], thixotropic behaviour, reaction kinetics, compressive strength
[34]	FA87.7%+GGBS4.6%+SF7.7%, FA83.1%+GGBS9.2%+SF7.7%, FA78.5%+GGBS13.8%+SF7.7%	NaOH+K_2SiO_3	1.8	L/b (0.49)	Attapulgite nano clay	River sand	1.1-1.9	Glass (0.25% by volume) Length: 4 mm	-	Static yield stress, structural build-up behaviour[b], thixotropic behaviour, shape retention ability, deformation under an increment load
[35]	FA80.6%+GGBS5.0%+SF14.4%	K_2SiO_3	2.0	L/b (0.4)	Thixotropic additive	River sand	1.72	-	-	Structural build-up behaviour[b], evolution of apparent viscosity, density, compressive strength[a], flexural strength[a], tensile strength[a], tensile bond strength
[52]	FA85%+GGBS15%	KOH+K_2SiO_3	1.8, 2.0	Act/b (0.35, 0.40), W/s (0.30, 0.35)	Attapulgite nano clay	River sand	1.5	-	Ambient temperature curing (23 ± 2 ºC)	Static yield stress, apparent viscosity, structural build-up behaviour[b], thixotropic behaviour, setting time, shape retention ability, build rate, compressive strength[a], reaction kinetics, microstructure
[53]	FA85%+GGBS15%, FA70%+GGBS30%,	KOH+K_2SiO_3	1.5	W/s (0.35)	-	River sand	0.85	-	Ambient temperature	Static yield stress, apparent viscosity, thixotropic behaviour,

	FA60%+GGBS40%									extrudability, buildability, compressive strength, microstructure
[54]	FA80%+OPC20%, FA77.5%+OPC20%+SF2.25%, FA75%+OPC20%+SF5%, FA65%+OPC35%, FA60%+OPC35%+SF5%, FA50%+OPC50%, FA47.5%+OPC50%+SF2.5%, FA45%+OPC50%+SF5%	Na_2SO_4	-	W/s (0.44)	-	River sand	1.35	-	-	Static yield stress, structural build-up behaviour[b], thixotropic behaviour, buildability
[43]	FA85%+LS15%, FA70%+LS30%, FA50%+OPC30%+LS20%, FA50%+GGBS30%+LS20%, FA50%+GGBS30%+LS19%+Al powder1%	NaOH+Na_2SO_4, NaOH+Na_2SO_4+Na_2SiO_3	-	L/b (0.27, 0.30, 0.35)	-	-	-	-	23 ± 1 ºC and >98% RH, 70 ºC for 24 h, 70 ºC for 48 h	Mini-slump, evolution of dynamic yield stress, plastic viscosity, setting time, open time, extensional rheology, extrusion rheology, compressive strength, flexural strength, porosity
[36]	FA70%+GGBS15%+SF15%, FA65%+GGBS20%+SF15%, FA60%+GGBS35%+SF5%, FA60%+GGBS30%+SF10%, FA60%+GGBS25%+SF15%	NaOH+Na_2SiO_3	-	L/b (0.18)	Nano-graphite platelet	River sand	0.55	-	60 ºC for 24 h, then ambient temperature (20 ºC)	Evolution of slump flow, dynamic yield stress, plastic viscosity, apparent viscosity, setting time, open time, shape retention ability, buildability, density, compressive strength, flexural strength, microstructure
[37]	FA100%, FA90%+GGBS10%, FA80%+GGBS20%, FA70%+GGBS30%, FA80%+GGBS10%+SF10%, FA70%+GGBS10%+SF20%, FA60%+GGBS10%+SF30%	Na_2SiO_3 (Anhydrous)	1.4	W/s (0.27)	ATTAGEL-50 (thixotropic additive)	Quartz sand	1.5	-	-	Dynamic yield stress, plastic viscosity, apparent viscosity, thixotropy, setting time, microstructure
[55]	GGBS100%	$Na_2SiO_3 \cdot 5H_2O$	-	W/s (0.32, 0.36)	Attapulgite nano clay, Hydromagnesite seed (nucleation seed)	Sand	0.83	-	-	Static yield stress, structural build-up behaviour[b], thixotropic behaviour, extrudability, buildability, microstructure

[46]	GGBS50%+CC50%	NaOH+Na_2SiO_3	1.7	W/s (0.28)	Sodium carboxymethyl starch (viscosity modifying admixture)	-	-	-	23 ºC and 90% RH	Slump flow, dynamic yield stress, plastic viscosity, water retention rate, setting time, compressive strength[a], flexural strength[a], drying shrinkage[a], porosity, microstructure
[15]	FA50%+GGBS50%	Na_2SiO_3 (GD grade), Na_2SiO_3 (Anhydrous), Na_2SiO_3 (GD grade)+Na_2SiO_3 (Anhydrous)	-	W/s (0.32-0.35)	Sucrose (retarder)	Silica sand	1.5	-	60 ºC for 24 h, then ambient temperature, Ambient temperature (23 ± 3 ºC)	Slump flow, dynamic yield stress, plastic viscosity, structural build-up behaviour[b], thixotropic behaviour, setting time, open time, extrudability, shape retention ability, buildability, density, compressive strength, flexural strength, porosity
[56]	FA50%+GGBS50%	Na_2SiO_3 (Anhydrous)	0.92	W/s (0.327, 0.335, 0.343)	Highly purified Magnesium Alumino Silicate (thixotropic additive), Sucrose (retarder)	Sand	1.5	-	Water	Apparent viscosity, structural build-up behaviour[b], thixotropic behaviour, elastic behaviour during printing, failure height of printed object, reaction kinetics
[44]	MK100%	NaOH+Na_2SiO_3	-	W/s (0.40-0.48)	-	-	-	-	-	Structural build-up behaviour[b], setting time, buildability
[27]	FA100%	NaOH+Na_2SiO_3	-	L/b (0.51-0.93)	-	Quartz sand	1.5	-	-	Structural build-up behaviour[c], setting time, open time, printability, interior structure using Xray μ-CT technique
[57]	FA75%+GGBS25%	NaOH+Na_2SiO_3 (D grade), NaOH+Na_2SiO_3 (N grade),	-	L/b (0.4)	Anhydrous borax (retarder), Sodium carboxymethyl cellulose	Sand	1.5	-	Ambient temperature	Extrudability, open time, shape retention ability, compressive strength

		$KOH+K_2SiO_3$ (KASIL 2040)			(viscosity modifying admixture)					
[58]	FA50%+GGBS50%	Na_2SiO_3 (Anhydrous)	0.90	W/s (0.32)	-	Sand	1.5	-	60 ºC for 24 h, then ambient temperature (23 ± 3 ºC)	Compressive strength, flexural strength, inter-layer strength
[38]	FA75%+GGBS15%+SF10%	$NaOH+Na_2SiO_3$	1.6, 1.85, 2.0	L/b (0.46)	Attapulgite nano clay	River sand	1.5	-	-	Thixotropic behaviour, structural build-up behaviour[c], tensile bond strength
[39]	FA80%+GGBS15%+SF5%	K_2SiO_3	1.18	L/b (0.45)	Magnesium aluminium silicate nano clay (thixotropic additive)	River sand	1.51	PVA (0.5% by weight) Length: 8 mm Diameter: 1.4 µm Stainless steel cable Diameter: 1000, 1500, 2000 µm	Ambient temperature	Thixotropic behaviour, flexural behaviour, microstructure
[50]	FA50%+GGBS50%	Na_2SiO_3 (Anhydrous)	1.0	W/s (0.40)	-	Silica sand	1.5	PVA (1.0% by weight) Length: 6 mm Diameter: 26 µm	Microwave, then 25 ºC and 50% RH	Structural build-up behaviour[b], thixotropic behaviour, inter-layer strength, inter-layer temperature, lateral deformation and stiffness, moisture content, microstructure, reaction kinetics
[40]	FA74%+GGBS16%+SF10%	K_2SiO_3	2.0	L/b (0.65)	Hydroxypropyl methylcellulose (thixotropic additive)	River sand	1.5	Glass (0.25-1.0% by volume) Length: 3, 6, 8 mm	Ambient temperature	Compressive strength, flexural strength, tensile strength
[47]	FA100%	$NaOH+Na_2SiO_3$ (D grade)	-	L/b (0.52)	-	Sand	1.0	Hooked-end steel (1.0% by volume) Length: 40 mm Diameter: 615 µm PP (0.5% by volume) Length: 5 mm Diameter: 22 µm	70 ºC for 2 h, then ambient temperature	Slump flow, flexural behaviour[a]
[41]	FA64%+GGBS25%+SF11%	$Na_2SiO_3 \cdot 5H_2O$	-	W/s (0.31)	Hydroxyethyl cellulose (viscosity	Silica sand	1.2	PP (0.56% by weight) Stainless steel cable Diameter: 1200 µm	-	Flexural behaviour

					modifying admixture)					
[42]	FA64%+GGBS25%+SF11%	$Na_2SiO_3 \cdot 5H_2O$	-	W/s (0.31)	-	Silica sand	1.2	Stainless steel cable Diameter: 1200 μm	20 ± 1 ºC and 95% ± 5% RH	Compressive behaviour, tensile behaviour, shear behaviour, pull-out behaviour
[51]	FA50%+GGBS50%	Na_2SiO_3 (Anhydrous)	0.9	W/s (0.28)	Sodium carboxymethyl cellulose (viscosity modifying admixture), Sucrose (retarder)	Sand	0.05	PVA (2.0% by volume) Length: 8 mm Diameter: 40 μm	23 ± 3 ºC for 24 h, then 60 ºC for 24 h, then ambient temperature	Density, compressive strength, flexural behaviour, porosity

Note: FA – fly ash; GGBS – ground granulated blast-furnace slag; SF – silica fume; MK – metakaolin; SS – steel slag; LS – limestone; CC – calcium carbonate; Al – alumina; L/b – liquid-to-binder ratio (the mass ratio of total liquid over the mass of solid from the binder); Act/b – activator-to-binder ratio (the mass ratio of liquid alkaline activator over the mass of solid from the binder); W/s – water-to-solid ratio (the mass ratio of total water over the mass of solids from the binder and alkaline activator); Agg/b – aggregate-to-binder ratio

[a]: Tests on mould-cast specimens only

[b]: By static yield stress test

[c]: By small amplitude oscillatory shear (SAOS) test

2.2. Processing steps

Fig. 2 presents the main printing process for extrusion-based 3DPG, which can be divided into mixing, pumping, extruding, and building. In general, the mixed material is transferred to the extruder via the pumping system to deposit the material layer by layer until the desired shape is achieved. To successfully print a geopolymer mixture on site, it is essential to control the quality of every process. As the processes are similar to those for 3D printed cementitious materials [5, 59, 60], only a brief overview of the extrusion-based processing steps for 3DPG is given here. Compared to robotic-based [13] and small-scale custom-made [51, 57] 3D printing systems, gantry-based 3D printing system [14, 15, 34, 35, 39] is widely used for geopolymers but often limited to vertical extrusion [5]. Robotic-based systems have more freedom in designing objects with various structures [20].

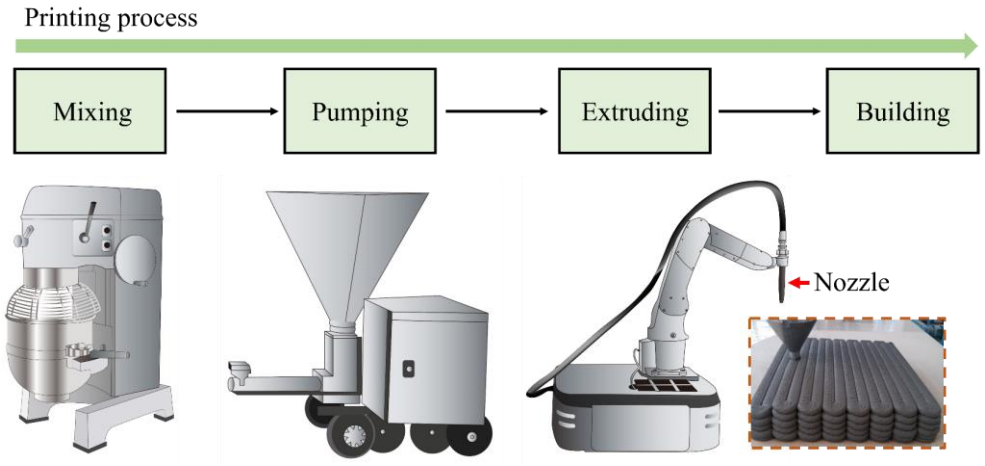

Fig. 2. Typical printing process for extrusion-based 3DPG [60, 61].

Batch mixing has been mainly used for 3DPG, where geopolymers are produced using either one-part or two-part mixing approach. Among them, one-part mixing system for geopolymers is more suitable for the in-situ work, where the solid alkaline activator is used during mixing instead of the prepared alkaline activator solution for the two-part mixing approach [12]. Handling a large quantity of alkaline solutions would reduce the safety of the construction working site and hence, two-part mixing system is now more preferred for precast application [62]. There is no consistent mixing protocol for 3DPG, and most studies started with mixing dry materials followed by the addition of liquid materials such as activator solution and water (if any). The adopted total mixing time of all existing studies ranged from 5 min to 15 min. It was reported that the solid alkaline activator was difficult to be completely dissolved if the total mixing time was less than 15 min [56]. To improve the dissolution of anhydrous Na_2SiO_3, after mixing all dry materials, Muthukrishnan et al. [56] added the water to the mixer at two different times with changing mixing speeds. To ensure an effective dispersion of some additives such as nano clay [55] and nano-graphite platelet [36], they were normally mixed with water before incorporating into the geopolymer matrix. Regarding 3DPG composites, short fibres were either mixed with the dry material [47, 56] or added after a homogenous

geopolymer matrix was reached [51]. It is worth noting that the sequence of fibre incorporation has a considerable effect on the fibre dispersion and orientation that would strongly affect the properties of resultant composites [63]. Until now, several studies [64-66] concluded that a longer mixing time can improve the flowability, mechanical properties, and durability of geopolymers. Alrefaei et al. [62] designed a new mixing method called "hybrid-mixing" that part of the mixing water is used to dissolve the solid activator while the rest is to dilute the chemical additive. They found that it can effectively enhance the flowability and compressive strength of FA-GGBS based geopolymers. However, to the best of the authors' knowledge, no research has been performed to explore the influence of mixing parameters on the engineering properties of 3DPG. These parameters would significantly affect the fresh and hardened properties, in particular printability. Thus, more studies are required to develop a consistent and effective mixing protocol for geopolymers used for 3D printing applications.

Pumping is an indispensable step in the delivery or transportation phase of 3D printing. Enough pressure is needed to transport the mixed material to the extruder. For small-scale applications or laboratory studies, the mixed material is always transported using a single pump with a short pumping distance [67]. This requires the material to undergo a fast structuration after the deposition. Large-scale printing work typically has a longer pumping distance and the print-head has extra space for the chemical additive (e.g., accelerator) to input prior to the extrusion [67, 68]. For 3DPG, different kinds of pumping systems have been utilised such as grout pump [13, 39], PFT swing M pump [15] and progressive cavity pump [40]. However, some issues may occur between pumping and material, which have been reported during the production process of 3D printed cementitious composites. For example, it was found that polymer fibres with a relatively long length may block the pump if the fibres are not well dispersed [60]. Therefore, ram [27, 43, 44, 50, 51, 58] or auger extruder [14, 15, 34, 36, 38, 41, 42, 45, 55, 56] were applied to avoid these potential issues. To date, it is still not clear which system is fully compatible for geopolymers without affecting the printing process and material properties, and thus further research is needed.

After the delivery or transportation phase, the material is ready for extrusion using the end part of the print-head known as nozzle that has different shapes such as circular, square, and rectangular. The shape, size, properties and fibre distribution of the extruded objects are largely influenced by the nozzle [60, 69]. The employed nozzle moving speed for 3DPG ranged from 3-120 mm/s, depending on the type and size of 3D printer and nozzle.

The extruded materials are deposited layer by layer until the final structure is built while the final printed object is susceptible to either plastic or elastic bulking failure (or a combination of both) due to the absence of mould or formwork [59, 60]. The deposited layer would experience the self-weight and process-induced forces from the upper layers, which may lead to plastic failure governed by the

yield strength (rheological parameter) of the extruded material [70, 71]. Moreover, another in-print failure mode (elastic bulking failure) can be triggered by the low yield strength (or stiffness) of the extruded material, the eccentric placement of the extruded layer, and a combination of both [72].

2.3. Printability requirements

As discussed in Section 2.2, each step during the 3D printing process can represent an aspect of printability which can be mainly divided into pumpability (delivery phase), extrudability (extrusion phase), open time (delivery and extrusion phases), buildability, and shape retention ability (building phase) [8, 60, 73]. These properties are governed by the fresh behaviour of 3DPG notably rheological behaviour. The general information on various printability properties is briefly discussed below as they have been widely reported by other existing review papers [2, 9, 59]. To date, there are still no standard methods for characterising the printability of 3DPG. Table 2 presents a summary of various parameters for characterising the extrusion-based 3DPG. The printability requirements of 3DPG will be discussed later.

Pumpability is defined as the ability of mixed material to go through the pumping system to the extruder without any blockage and negative impact on material properties [9, 73]. Ideally, when the mixed material is transported through the pumping pipe, a lubrication layer is formed on the pipe wall to improve the pumpability [74]. As indicated in Table 2, the existing studies characterised the pumpability of 3DPG using both yield stress and viscosity [15, 56]. Bong et al. [15] quantified the pumpability of 3DPG using the dynamic yield stress and plastic viscosity, which can be adopted as inputs to determine the required pressure for pumping the material based on the equation given in [75]. A better pumpability can be expected if the required pumping pressure was lower than the maximum conveying pressure for the used pump. Muthukrishnan et al. [56] applied the apparent viscosity of fresh geopolymers to determine the pumpability as the viscosity at the bulk can be used to evaluate the condition in the lubrication layer [76]. The static yield stress of fresh geopolymers was also used to estimate the pumpability of 3DPG [56]. As mentioned earlier, except for the rheology of bulk geopolymers, the properties of the lubrication layer cannot be ignored [2]. However, the rheological properties of the lubrication layer for 3DPG have not been studied and thus further studies are required to better characterise the pumping behaviour of 3DPG.

Extrudability is regarded as the ability of the material to extrude smoothly via the nozzle while retaining the original shape of the filament without apparent deformation, splitting and tearing [8, 9]. As shown in Table 2, the extrudability of 3DPG can be characterised by flowability, yield stress and viscosity [34, 43, 45]. When the static yield stress of fresh geopolymers was in the range of 600-1000 Pa, a smooth extrusion can be expected and the used rheometers could not offer enough torque for the measurement (i.e., poor extrudability) if the static yield stress exceeded this range [34]. Alghamdi et al. [43] printed the fresh geopolymers to assess the extrudability of 3DPG and revealed that

geopolymers had good extrudability when the printed samples exhibited little or no deformation. In addition, the flowability and dynamic yield stress of these mixtures were measured to determine the limits for these parameters. Within these limits, a smooth extrusion could be achieved. The extrudability of 3DPG is associated with the structure rebuilding ability determined using rheometers and a higher extrudability can be found if the geopolymers process a higher structure rebuilding ability [45]. Apart from the above parameters, the extrudability can also be evaluated through visual observation of the extrusion process of filament [53, 57] and the shape of extruded structure [15, 43], or by measuring the width of extruded filament [55].

In the delivery and extrusion phases, open time is another critical factor for 3D printing, which is defined as the time window that the material must be extruded [77, 78]. Beyond the open time, the material cannot be printed anymore. As seen in Table 2, the open time of 3DPG is normally determined by extruding the material at different times while the time that the material cannot be extruded is marked as the open time [15, 27, 36, 43, 57]. Moreover, the initial setting time and some rheological parameters can be also used to reflect the open time [13, 34, 35, 52].

During the deposition and building phases, buildability is the governing factor that is defined as the ability of deposited material to retain the shape and resist the load and deformation [9]. Aside from keeping the deposited shape, the bonding between the layers can also indicate buildability. Different parameters have been applied to characterise the buildability of 3DPG, while the commonly used ones are the recovery ability of apparent viscosity after subjected to a high shear rate, the evolution rate of static yield stress, and the integrity of final printed objects (Table 2). Panda et al. [34] simulated the printing process by applying different shear rates (0.1 s^{-1} and 100 s^{-1}) to the fresh geopolymers whilst the rheological test. The recovery ability of apparent viscosity after varying the shear rate from a high value (100 s^{-1}) to a low value (0.1 s^{-1}) was used to assess the buildability of 3DPG and a better buildability could be obtained when the recovery ability was higher. Similar approaches were adopted by other studies [50, 54, 56]. It was observed that the buildability of 3DPG was higher when the growth rate of static yield stress was larger [44, 55, 56]. Bong et al. [15] printed a column with a height of 940 mm (94 layers) to evaluate the buildability of 3DPG and observed very high integrity for the printed column, implying a higher buildability. Similar methods (but with different printed structures) were applied by other studies and other parameters (e.g., failure height of the printed structure) were used [36, 43, 56]. The shape retention ability listed in Table 2 can be considered as another important aspect of buildability for 3DPG, which can be quantified using a dimensionless number, called shape retention factor. For instance, Panda et al. [34] compared the cross-sectional area of fresh geopolymers inside a mould and the cross-sectional area after removing the mould. The difference between them was noted as the shape retention factor. Other parameters of characterising the shape retention ability are summarised in Table 2.

Although many different parameters with similar intrinsic origins have been utilised to characterise the printability of 3DPG, which are strongly related to the rheology of fresh geopolymers, especially yield stress and viscosity. For instance, when the integrity of the printed objects is used to assess the buildability, the key factors including initial yield stress and initial viscosity as well as the evolution of them can be considered. Prior to the assessment of buildability, sufficient pumpability, extrudability and open time should be achieved. It should be noted that most of the approaches mentioned above for characterising the printability of 3DPG are empirical, which cannot provide a comprehensive understanding of the intrinsic properties of 3DPG. Some studies only estimated certain rheological parameters of fresh geopolymers, while the samples were not printed. The results can only indirectly reflect the printability of geopolymers and thus it is vital to develop unified and standard test methods for each aspect of printability along with useful guidelines to improve the reliability of the test results and reduce the potential errors during each test.

In general, to successfully print an object, the pumpability, extrudability, open time, buildability, and shape retention ability should be adequate. The yield stress and viscosity should be as low as possible (i.e., high flowability) to ensure the mixed material can be easily transported to the extruder (good pumpability). Fresh geopolymers should possess moderate yield stress with low viscosity (i.e., adequate flowability) for acceptable extrudability to ensure a smooth extrusion process without dramatic damages to the extruded materials. Open time must be controlled to ensure there is enough time to complete the extrusion (i.e., sufficient setting time). Geopolymers should possess high static yield stress after the deposition to avoid potential failures mentioned in Section 2.2 (plastic and elastic bulking failures). Fig. 3a shows a typical evolution trend of yield stress for 3DPG, which can be mainly divided into four steps. Step 1 includes all processing steps before the extrusion like mixing and pumping and thus, the structuration of materials at this stage is very low or negligible. This can be attributed to the several rounds of high shearing with various magnitudes included in this stage, leading to a broken down of structuration [79]. Step 2 can be regarded as the deposition phase of materials and the initial static yield stress must be higher than $\rho g h$ where ρ and h are the density and thickness of the extruded filament, and g is the gravity of Earth [19]. During this stage, there exits primarily colloidal interactions between particles, leading to the formation of some early reaction products [79]. In step 3, a linear structural build-up (or green strength improvement) occurs due to the formation of bridges connecting the particles [79-81]. At this stage, most bridges between the particles are still weak and hence, the structural build-up is reversible if sufficient mixing is provided [19]. As the rigidification of percolated network of particles proceeds (step 4), the strength of printed materials evolves rapidly with an almost irreversible trend [19, 27]. According to [19], the static yield stress in the bottom layer should be higher than $\rho g H/\sqrt{3}$ (where H is the height of final printed object) to avoid the plastic failure shown in Fig. 3b. As mentioned earlier, the elastic bulking failure (Fig. 3c)

could occur due to the low yield strength of deposited material associated with low stiffness [71]. Thus, the risk of experiencing both failure modes can be reduced if the early-age yield strength of fresh geopolymers is high enough [71]. Moreover, printing configurations such as printing speed and printing layer cycle time also need to be controlled. Apart from these key printing requirements, other factors still need to be concerned. All these factors are related to and would affect each other during the printing procedure.

Table 2 Summary of parameters for characterising the printability of extrusion-based 3DPG.

Printability	Characterisation parameters	Remarks
Pumpability	Dynamic yield stress and plastic viscosity [15], static yield stress and apparent viscosity [56]	Better pumpability is found when the dynamic yield stress and plastic viscosity are lower [15] or when the apparent viscosity is in the range of 10-100 Pa·s and the static yield stress is below 5 kPa after the mixing of 45 min [56]
Extrudability	Specified rebuilding energy i.e., area between up-curve of each hysteresis loop and the corresponding equilibrium line [45], static yield stress [34], integrity of printed element during extrusion process or after extrusion [15, 43, 53, 57], mini-slump and dynamic yield stress [43], width of extruded filament [55]	Better extrudability is found when the specified rebuilding energy is higher [45] or when the static yield stress is in the range of 600-1000 Pa [34] or when no breakage or discontinuity of the extruded filament during the extrusion [53, 57] or when the printed element has an acceptable shape [15, 43] or when the maximum mini-slump and maximum dynamic yield stress are 9 mm and 700 Pa, respectively [43] or when the width of the extruded filament is close to the length of the nozzle [55]
Open time	Change of thixotropy over time i.e., area under the curve of torque against rotational speed [13], growth rate of static yield stress [34], growth rates of static yield stress and apparent viscosity [35], initial setting time [52], extrusion time after mixing [15, 27, 36, 42, 43, 57]	Longer open time is found when the growth rate of static yield stress is lower [34] or when the initial setting time is higher [52]
Buildability	Recovery ability of apparent viscosity after a high shear rate [34, 50, 54, 56], deformation after an incremental load of 0.1 N/s [34], observation of nozzle standoff distance of printed cylindrical structure [52], green strength [53], deformation of the bottom layer of printed cylindrical structure [54, 55], Integrity of printed structure [15, 36, 43, 44], growth	Better buildability is found when the recovery ability of apparent viscosity is higher [34, 50, 54, 56] or when the deformation of the printed object after an incremental load is lower [34] or when the nozzle standoff distance of the printed object is lower [52] or when the green strength is higher [53] or

	rate of static yield stress [44, 55, 56], elastic behaviour during printing [56], measured failure height of printed structure [56], lateral deformation under vertical load [50]	when the deformation of the bottom layer is lower [54, 55] or when the printed structure has higher integrity without obvious distortion [15, 36, 43, 44] or when the growth rate of static yield stress is higher [44, 55, 56] or when the elastic modulus of the object during the printing is higher [56] or when the measured failure height of the printed object is higher [56] or when the lateral deformation of the printed object under the vertical load is lower [50]
Shape retention ability	Shape retention factor i.e., ratio of cross sectional area before and after demoulding (or extruding) [34, 52] or ratio of top width to bottom width of printed sample [57], extrusion yield stress i.e. predicted by Benbow-Bridgewater model [43], measured height of each printed layer after 60 min (6 layers in total) [36], deformation of the sample under steel plates [15]	Better shape retention ability is found when the shape retention factor is higher [34, 52, 57] or when the extrusion yield stress is higher than 20 kPa [43] or when the deformation of the sample under steel plates is lower [15]

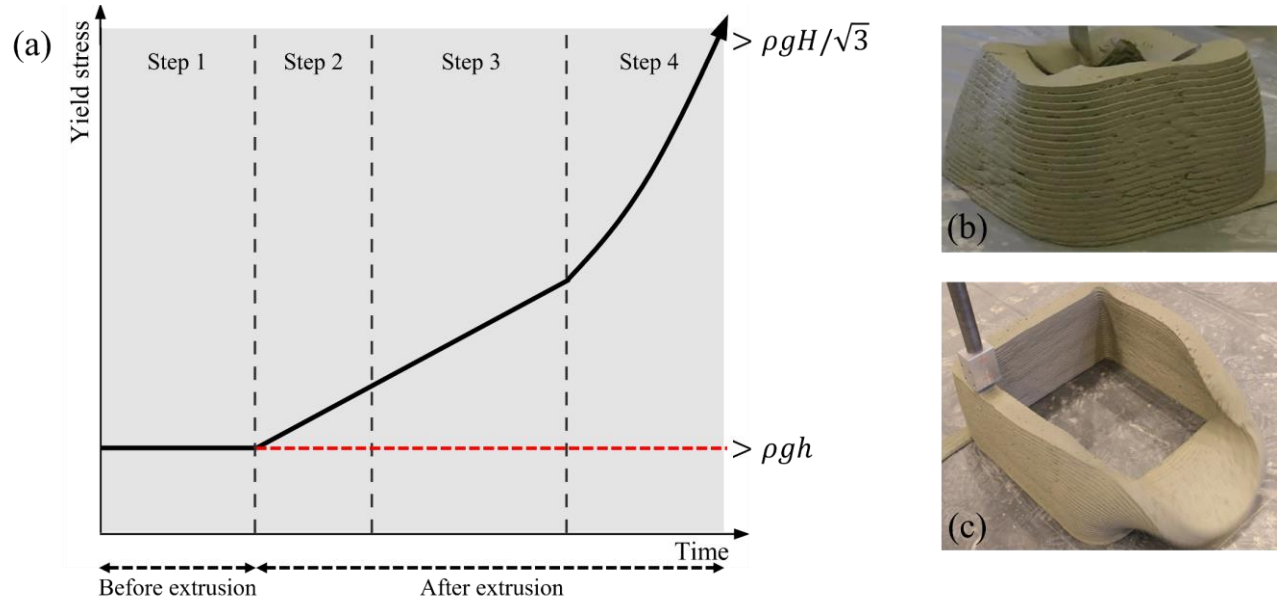

Fig. 3. Buildability requirements and failure modes: (a) required yield stress (based on [19, 27, 80]), (b) plastic failure mode [70], and (c) elastic bulking failure mode [70].

3. Fresh properties of 3D printed geopolymers

3.1. Flowability and its relation to printability

Sufficient flowability is crucial for the applicability of geopolymers as poor flowability can lead to poor compaction, excessive void formation and reduced hardened properties. Regarding 3D printing, geopolymers could be easily transported via the pumping system to the extruder if they exhibit

relatively high flowability. Flowability can be measured using either mini-slump test [43] or flow table test [15]. The effects of different factors such as replacement binder, activator, and additive on the flowability of 3DPG have been increasingly studied, the results of which are illustrated in Fig. 4.

Fig. 4a presents the effects of different alternative binders including LS, GGBS, SF, OPC and alumina (Al) powder on the flowability of geopolymers for 3D printing. The limited data shown in Fig. 4a shows that the presence of LS, SF and Al powder can increase the flowability of geopolymers [36, 43], while the incorporation of GGBS adversely affected the flowability [36]. For instance, the mini-slump of FA-LS based geopolymers slightly went up with the increasing LS dosage from 15% to 30% [43], mainly due to the reduced contact between the reactive particles [82]. However, the effect of replacing FA with LS on the flowability of geopolymers cannot be confirmed as the activator content was not constant when the LS dosage changed. Similarly, although it was reported that replacing SF with 1% Al powder can improve the mini-slump of geopolymers, such improvement could be caused by the combined effect of Al powder and activator [43]. As shown in Table 2, the mini-slump can be used to reflect the extrudability and Alghamdi et al. [43] found that a smooth extrusion was found when the mini-slump of fresh geopolymers was less than 9 mm. Due to the accelerated reaction and increased number of angular particles [83, 84], it was found that the slump flow of geopolymers can be reduced by 6.3% if replacing FA with GGBS while keeping the SF content constant (Fig. 4a) [36]. By contrast, replacing GGBS with SF led to an increased slump flow (4.1-7.3%) [36]. Previous studies observed that when the added SF content is lower than the critical dosage, SF would act as a lubricator to improve the flowability of geopolymers, while an opposite effect occurs if the dosage is beyond the critical dosage [85-87]. The 'resting time=5 min' in Fig. 4a means that the slump flow was obtained by conducting the flow table test 5 min after the first test and the slump flow of geopolymers slightly increased as the resting time rises (0-15 min), which contradicts the fact that the flowability should be smaller as the reaction proceeds [36]. Thus, to further explain this phenomenon, repetitive tests are required.

Apart from binders, activator type also has a strong influence on the flowability of geopolymers. The slump flow of FA-GGBS based geopolymers was found to be only 105 mm when the anhydrous Na_2SiO_3 with a modulus (SiO_2/Na_2O) of 0.9 was used as the activator (Fig. 4b), which can be ascribed to the rapid reaction kinetics of anhydrous Na_2SiO_3 [15]. To address this issue, the GD grade Na_2SiO_3 was used to partially replace the anhydrous Na_2SiO_3, indicating that replacing 25% anhydrous Na_2SiO_3 with GD grade Na_2SiO_3 can improve the slump flow by 25.8% due to the increased modulus of the activator, resulting in a reduction in yield stress while such effect becomes more pronounced when the activator modulus is below 1.2 [15]. However, taking the pumpability into account, they suggested that the highest replacement ratio of anhydrous Na_2SiO_3 should be limited to 50% as beyond this ratio, the synthesised FA-GGBS based geopolymers were difficult to pump [15].

As mentioned in Section 2.1, different kinds of additives were utilised to tailor the printability of geopolymers via changing their fresh properties such as flowability. As shown in Fig. 4c, it can be found that the incorporation of sodium carboxymethyl starch (viscosity modifying admixture) can considerably reduce the slump flow of FA-CC based geopolymers [46], where the reduced flowability was found to help mitigate the deformation of geopolymers after the extrusion, improving the buildability. Bong et al. [15] revealed that the incorporation of 0.5% sucrose (retarder) can increase the slump flow from 105 mm to 120 mm mainly due to the delayed reaction process of geopolymers after the usage of sucrose, while further addition of sucrose (1.0%) did not show any positive influences.

Regarding the effect of fibre type on the flowability of geopolymers for 3D printing, there is only one study [47] available which indicated that adding 0.5% (by volume) polypropylene (PP) fibre led to a lower flowability of geopolymers than the incorporation of 1.0% steel fibre. Due to the contact network between fibres and matrix, the flowability is generally decreased after the addition of fibres [88], and the reduction degree of flowability is strongly affected by the critical fibre dosage, depending on the fibre properties [63]. The critical fibre dosage of PP fibre may be lower than that of steel fibre [89] and hence, the flowability of geopolymers containing PP fibres is smaller. Nevertheless, the printability related properties of these fibre reinforced geopolymer composites were not assessed in [47], and thus the feasibility of using these fibres for 3D printing applications is still unclear.

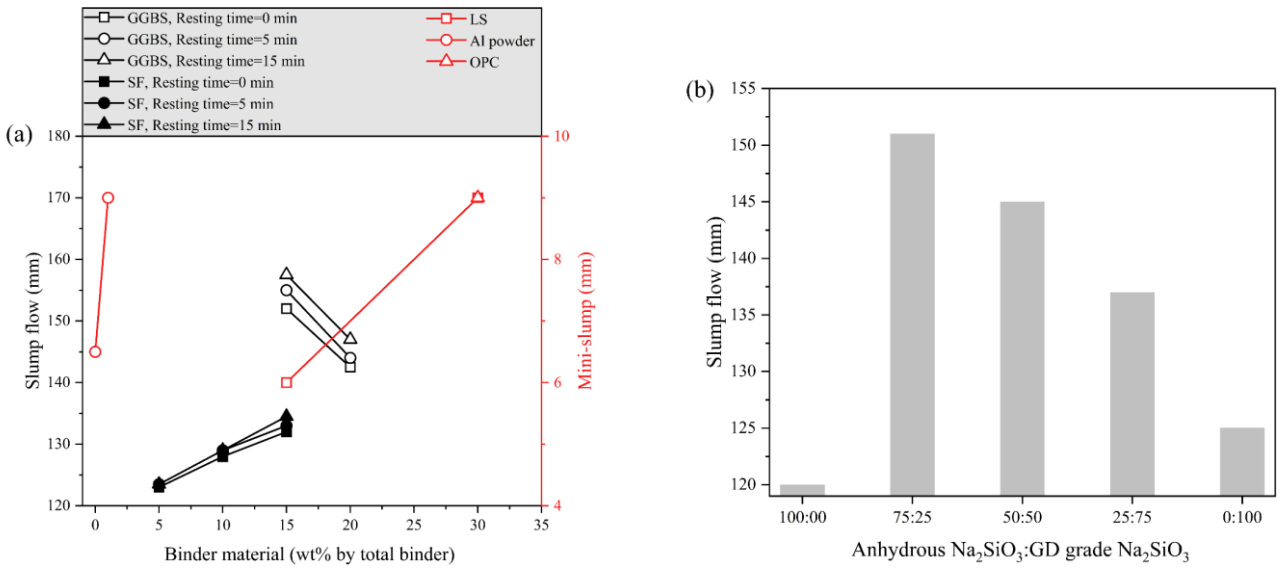

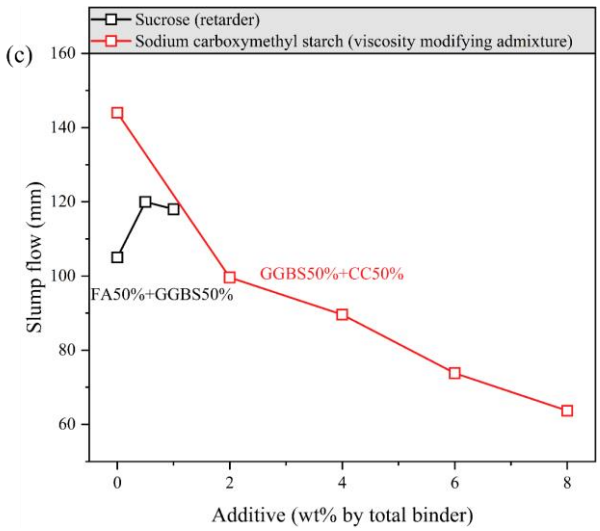

Fig. 4. Flowability of fresh geopolymers for 3D printing: (a) effects of binder type and content, (b) effect of activator type, and (c) effect of additive content (adapted from [15, 36, 43, 46]).

3.2. Setting time and its relation to printability

Setting time can reflect the hardening evolution of geopolymers, which is usually evaluated using Vicat needle test and also can be determined through rheological measurement [90]. Based on the penetration depth during the Vicat needle test, setting time can be categorised as initial and final setting time. If the setting time is not well controlled, it may adversely affect the delivery, extrusion and building phases, especially open time. Based on the existing research (Table 1), the effects of replacement binder (GGBS, SF, OPC, Al powder), activator and additive (nano clay, sodium carboxymethyl starch and sucrose) on the setting time of geopolymers were estimated, the results of which are depicted in Fig. 5.

As seen in Fig. 5a, the initial setting time of geopolymers prolonged as the increase of either LS or Al powder content, or as the decrease of GGBS dosage. For instance, the initial setting time of geopolymers was reduced from 151 min to 18 min with the increase of GGBS content from 0% to 30% [37], due to the high calcium content of GGBS that accelerates the reaction to form C-A-S-H and N-C-A-S-H gels (if in association with FA) [91, 92]. Besides, the combined effect of LS (or Al powder) and activator led to an obvious increase in the initial setting time of geopolymers, which accordingly prolonged the open time from 60 min to 180 min [43]. It can be suggested that to ensure a satisfactory open time for 3DPG, it is crucial to select an appropriate binder proportion.

It was reported that combining two different kinds of activators (anhydrous Na_2SiO_3 and GD grade Na_2SiO_3) can not only improve the flowability but also address the issue of short setting time for geopolymers activated with sole anhydrous Na_2SiO_3 [15]. As indicated in Fig. 5b, when anhydrous Na_2SiO_3 was used to activate FA-GGBS based geopolymers, the initial and final setting time were only 65 min and 96 min, respectively, which could not meet the requirement for 3D printing [15]. When another Na_2SiO_3 (GD grade) with a higher modulus was incorporated, the setting time was

increased considerably. For instance, the setting time of geopolymers activated by only GD grade Na_2SiO_3 exceeded 480 min. Fig. 5c shows that the setting time of FA-based geopolymers increased with the rising L/b [27]. A comparison between the open time determined from the extruded samples with different L/b and its initial setting time suggests that the open time was extremely shorter than the initial setting time [27]. Fig. 6 shows some images of the extruded samples taken by digital camera and X-ray micro-CT. As observed, when the open time was exceeded, the samples were difficult to extrude with poorly formed shapes (Fig. 6a), and many defects can be observed inside the non-extrudable samples, as illustrated in Fig. 6b.

Fig. 5d shows that the use of sucrose can improve the setting time, as reported in [15]. Besides, as seen in Fig. 5d, incorporating sodium carboxymethyl starch can help prolong the setting time of geopolymers due to the delayed reaction process through the attachment on the surface of binder particles [46]. This effect was found to be more apparent when the surrounding temperature was lower. On the other hand, Panda et al. [52] found that the incorporation of nano clay had a trivial impact on the setting time of geopolymers that the initial setting time was increased from 19 min to 22 min only when 1.5% nano clay was added (see Fig. 5d)

Based on the above results and discussion, it suggests that the initial setting time could be used to tailor the printability window (open time), while a limit should be set to maintain adequate flowability for pumping. However, a longer setting time may lead to a higher flowability for mixtures and thus, segregation may happen which weakens the lubrication layer during the pumping. It is helpful to evaluate the empirical relationships between initial setting time and open time for getting more insights into the control of printability window.

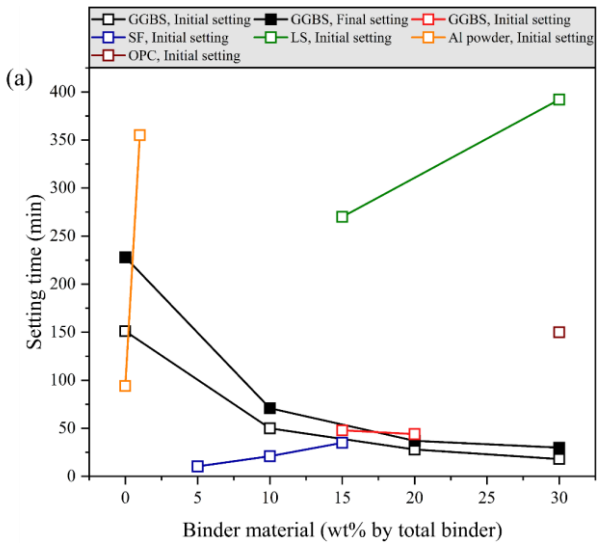

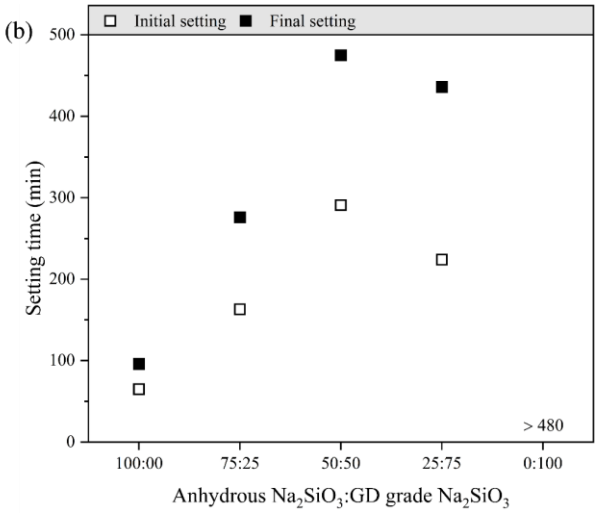

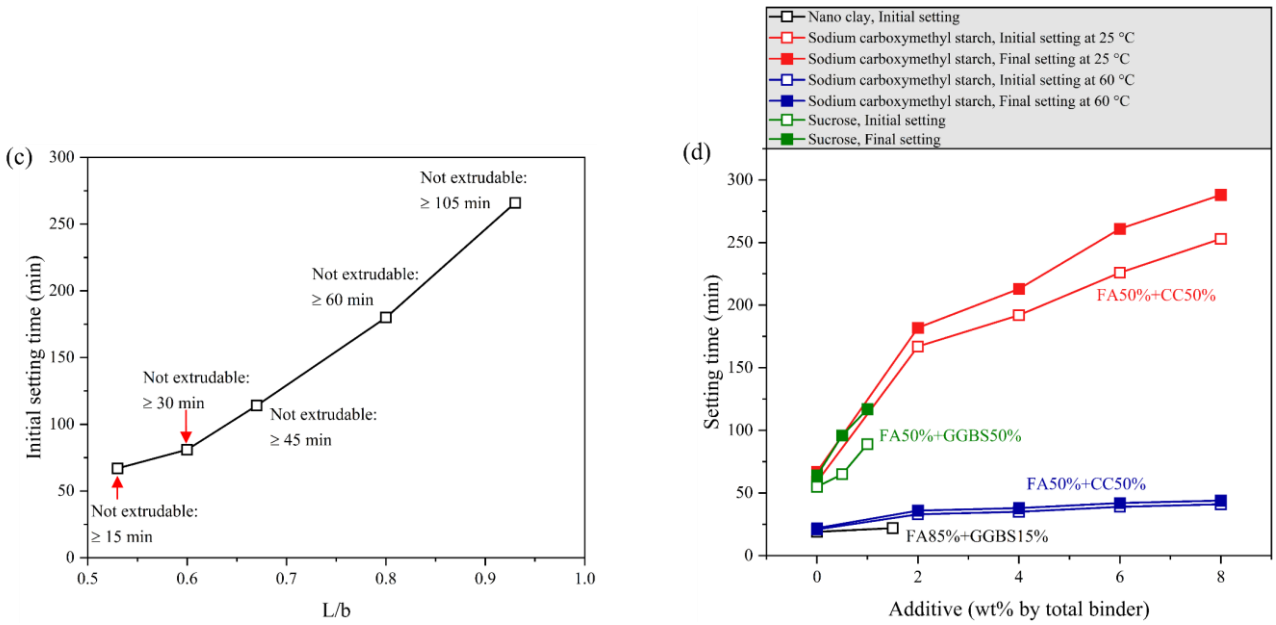

Fig. 5. Setting time of fresh geopolymers for 3D printing: (a) effects of binder type and content, (b) effects of activator type, (c) effect of liquid-to-binder ratio (L/b), and (d) effect of additive content (adapted from [15, 27, 36, 37, 43, 46, 52]).

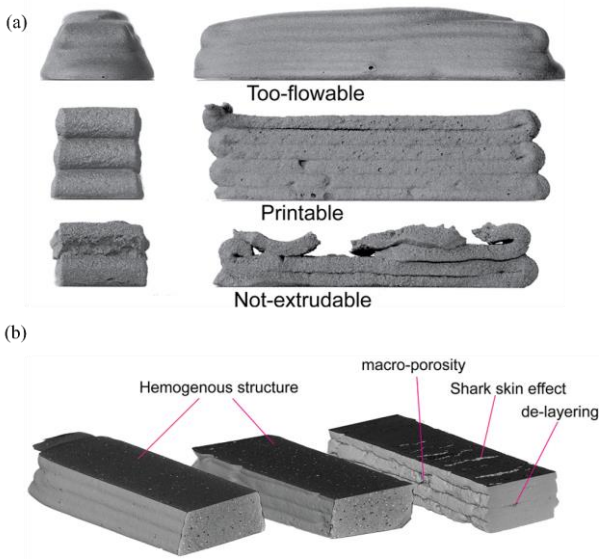

Fig. 6. Examples of some extruded geopolymers [27].

3.3. Yield stress and viscosity and their relations to printability

As aforementioned, yield stress and viscosity of fresh geopolymers have strong effects on their printability, which can be determined by a rotational rheometer (Fig. 7a). Fig. 7b and c display the testing protocols for measuring the above parameters. Static yield stress is defined as the minimum shear stress to initiate the flow of materials, which can be generally determined by applying a constant shear rate (0.01-0.5 s^{-1} [14, 44, 52-55]) to the test specimens (Fig. 7b) [93]. It is worth noting that a pre-shear stage with an extremely high shear rate (e.g. 60 s^{-1}) is normally required to remove the shearing history and bring the test specimens back to the reference state [94, 95]. Dynamic yield stress is regarded as the required shear stress to maintain the flow of materials while plastic viscosity is

noted as the resistance of materials to the flow, which can be evaluated using the testing protocol shown in Fig. 7c. Afterwards, a rheological model (e.g., Bingham model) is used to fit the flow data and thus, the dynamic yield stress and plastic viscosity can be obtained.

As stated in Section 2.3, to ensure smooth delivery and extrusion processes, the yield stress and viscosity before the deposition should be as low as possible. For different 3D printing systems, the limits of yield stress and viscosity can vary. Fig. 8a shows the effect of replacement binder content on the static yield stress and apparent viscosity of geopolymers for 3D printing. Generally, as seen, increasing either GGBS or OPC content raised both static yield stress and apparent viscosity of geopolymers, while increasing the FA dosage caused opposite changing trends [53, 54]. Besides, replacing 10% FA with SF increased the static yield stress by about 103.3% without affecting the extrudability of geopolymers, and the shape retention ability was improved in the presence of SF, as reported by [14].

Both Act/b (or W/s) and activator modulus have dramatic influences on the static yield stress and apparent viscosity of geopolymers (Fig. 8b). If the solid activator is used, the activator dosage and water content need to be carefully selected to ensure the mixture is pumpable and extrudable. Panda et al. [53] found that when the activator dosage of solid KOH and K_2SiO_3 changed from 10% to 15% (by mass of the total binder) while keeping W/s as 0.35, the static yield stress of FA-GGBS based geopolymer exhibited a negligible change, while an approximately 25.4% increase in static yield stress can be observed when the activator dosage went up to 20%. In this study, W/s was kept constant and the total water content in the mixture reduced with the increasing activator dosage. Thus, with the increase of activator dosage, a higher pH and ionic strength of surface charges can be formed, leading to an increased static yield stress [53]. A consistent finding was reported in [56] that adjusting the dosage of anhydrous Na_2SiO_3 from 7.5% to 10% (by mass of the total binder) while keeping the total water content constant, the static yield stress of FA-GGBS based geopolymer was enhanced by 18.5 times due to the rapid dissolution of the solid activator [15, 96]. It should be noted that the water content in this study was not altered as the increase of activator dosage and thus, W/s of the mixture reduced accordingly, which can be seen in Fig. 8b that the static yield stress of geopolymers increased with the decreasing W/s [56]. Therefore, the critical dosage of anhydrous Na_2SiO_3 can be regarded as 7.5% as exceeding this dosage may make the mixture difficult to extrude due to the extremely high static yield stress immediately after the mixing [56]. However, when the dosage of anhydrous Na_2SiO_3 was 7.5% (equivalent to W/s of 0.335), the static yield stress of fresh geopolymers was only 94 Pa and the corresponding buildability was very low [56]. Muthukrishnan et al. [56] used the failure height of printed samples to reflect the buildability (Fig. 9). When the static yield stress of geopolymers was less than 100 Pa, the printed samples failed at the height of 6 layers. On the other hand, as displayed in Fig. 8b, increasing the Act/b of geopolymers activated by liquid KOH and

K_2SiO_3 declined both static yield stress and apparent viscosity of FA-GGBS based geopolymers [52], which can be ascribed to the delayed saturation-polycondensation stage and reduced hardening speed [97]. Similar results were reported in [98, 99] that the static yield stress of fresh geopolymers increases with the reducing W/s or Act/b, independent of the solid or liquid activator used. Moreover, regardless of Act/b, it was observed that the static yield stress of geopolymers was increased by 4.8-6.8 times with the increase of activator modulus from 1.8 to 2.0 [52] (Fig. 8b). As explained in Section 3.1, the activator with a modulus below 1.2 can bring plasticising effect to reduce the yield stress while this effect vanishes when the modulus is over 1.4 [85]. Fig. 8b shows that the apparent viscosity of geopolymers also raised with the increasing activator modulus, due to the increasing number of colloidal clusters [52, 85]. Given the increased static yield stress and apparent viscosity, the shape retention factor was found to be increased by 2.71 times, leading to a better shape retention ability for geopolymers [52]. Even so, this result was obtained based on the extrusion of a single filament, which cannot reflect the true buildability of geopolymers. Hence, Panda et al. [52] assessed the nozzle standoff distance (i.e. distance between the upper part of the extruded layer and the nozzle) to characterise the buildability of geopolymers and found that when the activator modulus was 2, the nozzle standoff distance of the mixtures increased with the increasing printing layer. This can be attributed to the slow structural build-up, implying that the static yield stress of the bottom layers was not sufficient to withstand the stresses from the upper layers and the printing processes.

Several types of additives were applied to adjust the yield stress and viscosity for improving the printability of geopolymers (Fig. 8c). The commonly used one was nano clay (0.2-0.6%) that had an apparent effect on the static yield stress [52, 55]. For instance, Panda et al. [55] revealed that the addition of 0.6% nano clay increased the static yield stress of geopolymers by 6.7 times, which could be due to the dense internal network induced by the edge to face interaction of nano clay particles [49, 100]. With the inclusion of 0.5% nano clay, the buildability of geopolymers was found to be improved as no visible nozzle standoff distance was observed [52]. However, as seen in Fig. 8c, the increment effect in static yield stress by nano clay was not pronounced when the Act/b of the mixture was higher owing to the reduced interaction of nano clay under high pH solution [52, 101]. Compared with its influence on static yield stress, the effect of nano clay on the apparent viscosity of geopolymers was less conspicuous (Fig. 8c), which can be associated with the reduced viscosity of nano clay under high shearing [49]. Panda et al. [55] applied both nano clay and hydromagnesite seed to tailor the printability of geopolymers and found that the addition of 2% hydromagnesite seed led to a 36.5% rise in the static yield stress of geopolymers compared to geopolymers containing solely nano clay. A slender column without any apparent deformations that was made of the mixtures incorporating 0.4% nano clay and 2% hydromagnesite seed was successfully printed [55]. It was indicated that using the printing speed of 90 mm/s can achieve the highest extrudability based on the

width of extruded filaments, and the buildability was acceptable when using this printing speed [55]. To improve the extrudability of the anhydrous Na_2SiO_3 activated geopolymer mixtures by lowering the static yield stress, 1.0% sucrose was added in [56]. However, the buildability was still unacceptable as the printed samples failed at the height of 58 layers, as displayed in Fig. 9. By combining another thixotropic additive (highly purified Magnesium Alumino Silicate) and 1.5% sucrose, the buildability of geopolymers was significantly improved as the printed samples did not fail up to 120 layers [56]. Although the initial static yield stress of this mixture was comparable to that containing 1.0% sucrose (approximately 730 Pa), the buildability was significantly improved. This implies the importance of assessing the structural build-up of 3DPG which will be discussed further in Section 3.4.

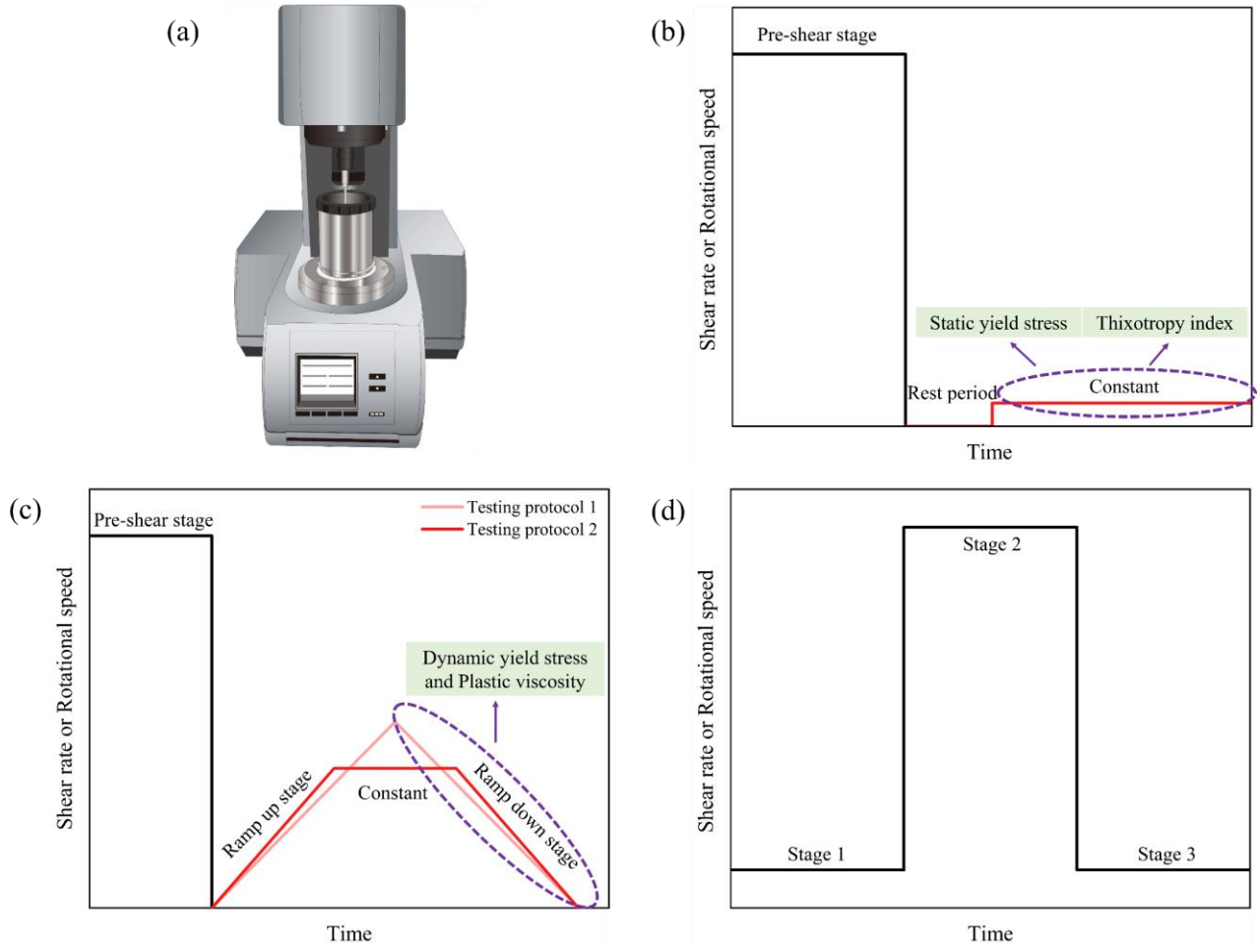

Fig. 7. Testing protocols for estimating the rheology of geopolymers (based on [34, 37, 93, 102, 103]).

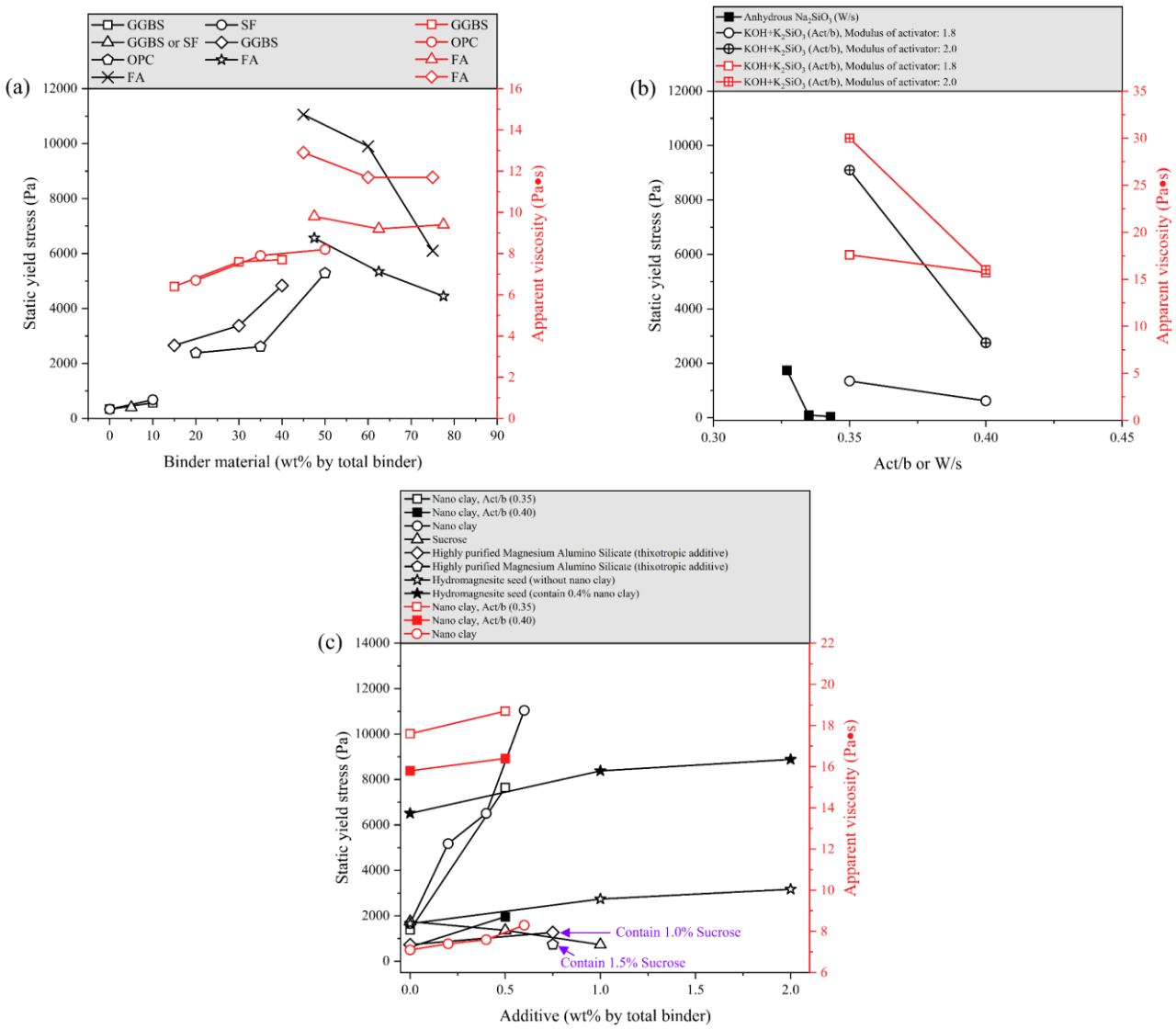

Fig. 8. Static yield stress and apparent viscosity of fresh geopolymers for 3D printing: (a) effects of binder type and content, (b) effect of Act/b (activator-to-binder ratio) or W/s (water-to-solid ratio), and (c) effect of additive content (adapted from [14, 52-56]).

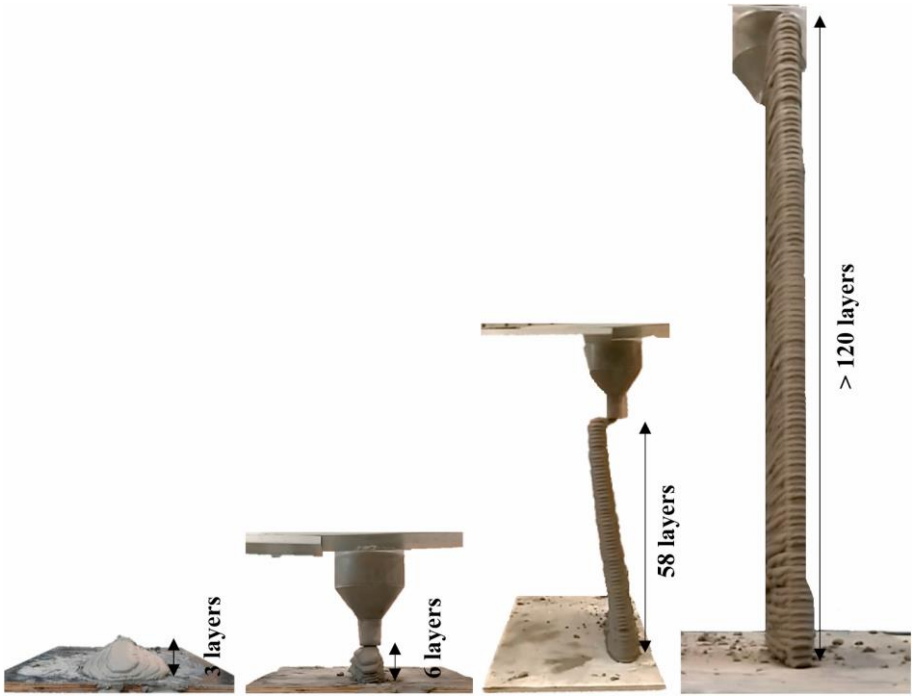

Fig. 9. Examples of some buildability assessments for 3DPG [56].

The effect of various binders (LS, Al powder, OPC, GGBS and SF) on the dynamic yield stress and plastic viscosity of geopolymers for 3D printing are shown in Fig. 10a. As seen, the dynamic yield stress and plastic viscosity of geopolymers were reduced by 69.6% and 54.7%, respectively when the LS replacement dosage changed from 15% to 30% [43], which can be ascribed to the filling role and water retention ability of LS, and the plasticising effect of activator [43, 85, 104]. Replacing FA with LS improved the buildability of geopolymers and at the 30% replacement, the printed samples with hollow structures did not show any layer deformations [43]. They also found that the mixtures containing 1% Al powder possess adequate printability without significantly changing the dynamic yield stress and plastic viscosity. Guo et al. [37] explored the effects of replacing FA with GGBS or SF on the dynamic yield stress and plastic viscosity of geopolymers using two rheological models, i.e., Bingham model and Herschel-Bulkley model. Regardless of binder type, both models can fit the flow behaviour well with R^2 over 0.99. Besides, they concluded that replacing 10% FA with SF can achieve an optimal printability as this mixture exhibited high dynamic yield stress (103.97-106.97 Pa) and adequate plastic viscosity (8-8.12 Pa·s) to have sufficient extrudability and ability to retain the printed shape (Fig. 10a). However, the bonding condition of printed samples was still a concern based on SEM micrographs, which may negatively affect the hardened properties. Zhang et al. [45] found that the dynamic yield stress of geopolymers increased with the decrease of activator modulus (1.0-0.5), which can be seen in Fig. 10b. The authors attributed this increase to the accelerated reaction of aluminosilicate material due to the increasing number of Na ions [105].

Fig. 10c illustrates the dynamic yield stress and plastic viscosity of geopolymers in relation to additives. As seen, increasing the nano-graphite platelet did not have a consistent effect on both

dynamic yield stress and plastic viscosity, and using 0.5% nano-graphite platelet can lead to the highest values and thus the best buildability for 3DPG [36]. On the other hand, Sun et al. [46] reported that the addition of sodium carboxymethyl starch can increase both dynamic yield stress and plastic viscosity of GGBS-CC based geopolymers, where the improved plastic viscosity can help avoid the segregation during the pumping and the enhanced dynamic yield stress can prevent the printed samples from collapsing.

As discussed above, the initial yield stress and viscosity can strongly influence the pumpability and extrudability of geopolymers, while the suitable ranges for them have been rarely explored. Thus, for future research, the applicable ranges of initial yield stress and viscosity should be determined for different mix proportions and 3D printing systems.

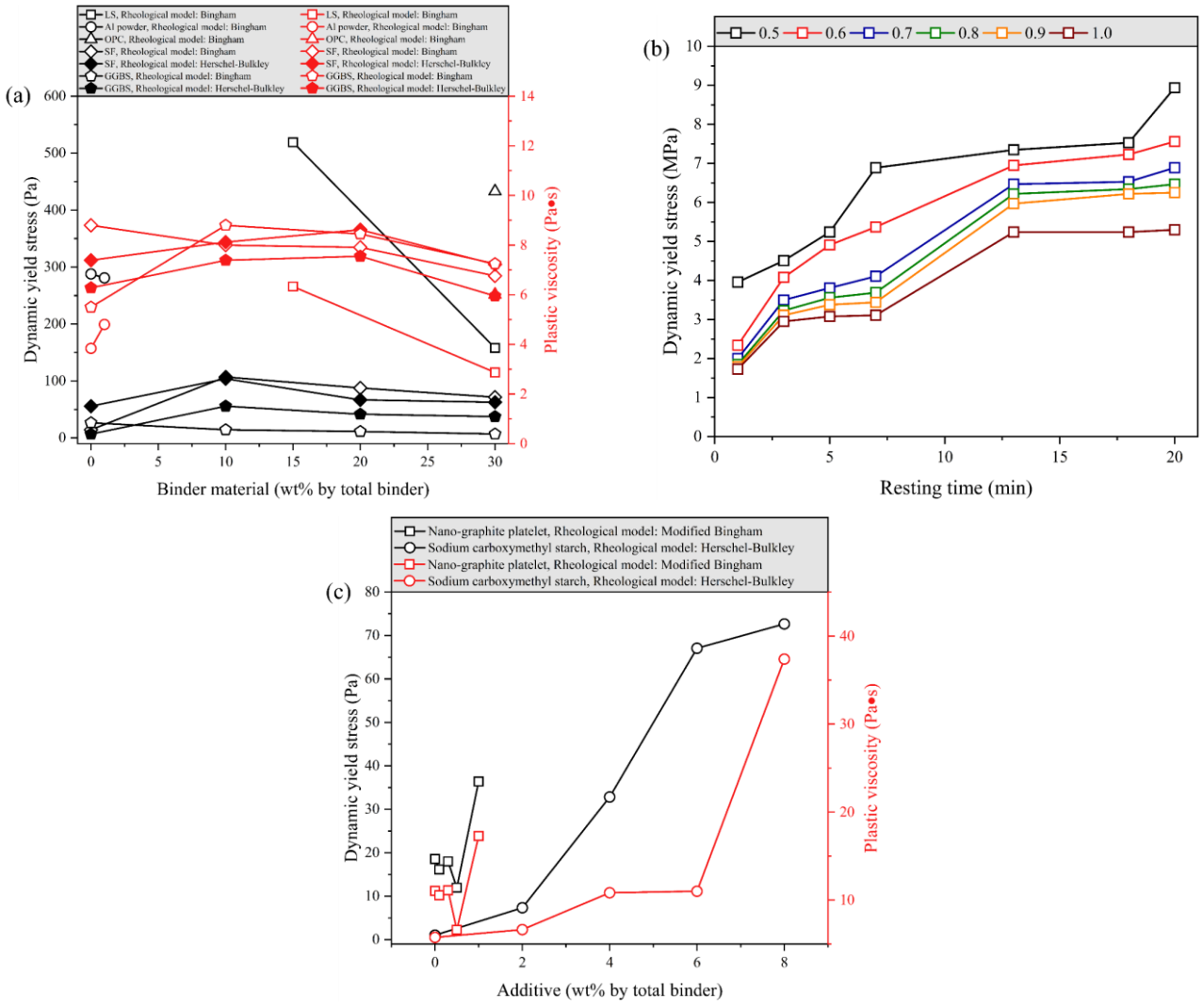

Fig. 10. Dynamic yield stress and plastic viscosity of fresh geopolymers for 3D printing: (a) effects of binder type and content, (b) effect of activator modulus, and (c) effect of additive content (adapted from [36, 37, 43, 45, 46]).

3.4. Structural build-up and its relation to printability

The structural build-up is an imperative parameter for 3D printing of materials especially during the building phase that can be determined using either the static yield stress test or small amplitude

oscillatory shear (SAOS) test [93]. Regarding the former one, it measures the static yield stress after specific intervals of time (resting time). For the SAOS test, the tested sample is typically subjected to a continuous shear strain to monitor the rheological properties (e.g., storage modulus and loss modulus) within the linear viscoelastic domain [93, 106]. The current research has been mainly focused on the effects of binder and additive on the structural build-up behaviour of geopolymers for 3D printing, the results of which are presented in Fig. 11.

Fig. 11a demonstrates the structural build-up behaviour (increase rate of static yield stress) of geopolymers considering different types of binders. It can be observed that replacing FA with GGBS improved the structural build-up behaviour of geopolymers (square and rhombic symbols in Fig. 11a) because of the faster chemical reaction rates [14, 34]. Panda et al. [34] related the growth of static yield stress to the open time of geopolymers that the open time of mixtures containing 15% GGBS was around 20 min, while 30 min was found for mixtures incorporating 10% or 5% GGBS (rhombic symbols). Similarly, the development of static yield stress was also used to evaluate the open time in [35]. As seen in Fig. 11a, the static yield stress of the mixture (circular symbols) changed considerably after 20 min, where this time was regarded as open time by [35]. Panda et al. [14] observed that replacing FA with SF did not change the increase rate of static yield stress (circular symbols), while the structural build-up behaviour of geopolymers reduced with the increasing FA dosage due to the slow chemical reaction rate and micro-filling influence of FA (triangular symbols) [34, 54, 93].

As discussed in Section 3.3, increasing the content of anhydrous Na_2SiO_3 (5%-10%) led to an increased initial static yield stress for FA-GGBS based geopolymers [56]. Similar effects have been captured for structural build-up behaviour. It was found by the same study [56] that the mixtures with an activator content of 10% had static yield stress of over 5000 Pa after 10 min resting time, which cannot be extruded anymore. Contrarily, the increase rates of static yield stress for mixtures with an activator dosage of 5% and 7.5% were much lower, where the static yield stress values were in the range of 1000-2500 Pa after 45 min resting time. However, as mentioned earlier, poor buildability was observed for these mixtures (Fig. 9).

As seen in Fig. 11b, independent of binder type, the addition of nano clay (0.4%-0.5%) did not lead to a higher increase rate of static yield stress, while the evolution was more stable compared to that without nano clay [52, 55]. It was found that the increase in static yield stress induced by the incorporated nano clay appears at the very beginning (i.e. resting time is zero), implying that the influence of nano clay on the structural build-up behaviour is strongly associated with the colloidal interaction between particles [49, 79, 107, 108]. It is worth mentioning that the risk of encountering pumping and extrusion issues may be lower if the growth of static yield stress is stable for printing materials. Bong et al. [15] applied 0.5% sucrose to reach a stable growth rate of static yield stress (triangular symbols), which offered sufficient extrudability and open time for the printing work, as

well as adequate static yield stress to withstand the stress from up to 120 deposited layers. Similarly, to ensure a sufficient open time while maintaining the buildability, Muthrkrishnan et al. [56] incorporated 1.5% sucrose to reduce the growth rate of static yield stress caused by the presence of highly purified Magnesium Alumino Silicate. This explains why this mixture performed best during the buildability test (Fig. 9), primarily because of the more stable structural build-up (Fig. 11b).

As aforementioned, the SAOS test is another method to characterise the structural build-up behaviour of geopolymers. Panda et al. [38] reported that the storage modulus of geopolymers declined with the increasing activator modulus ($NaOH+Na_2SiO_3$) from 1.6 to 2.0, implying a slower structural build-up behaviour. The open time of geopolymers with a higher structural build-up was shorter, which may affect the hardened properties, especially bond strength. As stated in Section 3.3, during the rheological tests, pre-shearing is needed to eliminate the shearing history of tested samples, while this has been challenged by Feys et al. [109] that pre-shearing may create different rheological properties for the tested samples. Thus, Ranjbar et al. [27] studied the effects of different pre-shearing conditions on the rheological properties of FA-based geopolymers to develop a reliable and accurate rheological testing protocol for 3DPG. They reported that whilst the SAOS test, the applied pre-shearing magnitude should be larger than the critical strain of breaking the internal structure of tested samples to remove all the shearing history. Besides, they found that the static yield stress can be predicted using the storage modulus, which can be used to quantify the printability of FA-based geopolymers.

Structural build-up behaviour is important for deposited geopolymer samples after extrusion. However, it may affect other aspects of printability, e.g., open time. To obtain satisfactory pumpability, extrudability and open time while keeping enough buildability, the growth rate of static yield stress (or storage modulus evolution rate) should be lower during the delivery and extrusion phases but must be higher during the building phase. It is worth noting that most existing studies on 3DPG tailored the structural build-up behaviour by adjusting the mix design during the mixing stage, especially through the addition of additives (Fig. 11b). However, in this way, it is difficult to accurately and timely obtain the required rheological properties in different printing steps. Thus, an increasing number of studies have attempted to develop effective set-on-demand approaches for 3DPG. Unlike the conventional method, the so-called set-on-demand retards the mixture at the initial mixing stage (increased setting time) and improves its structural build-up behaviour at the print-head using a certain type of accelerator, e.g., shotcrete accelerator [71, 110, 111]. As such, the required yield strength can be well achieved just after the deposition, which helps enhance the buildability of 3DPG [71]. A new print-head design for set-on-demand geopolymers via adding the activator in multiple stages was proposed in [71], as illustrated in Fig. 12. Given the limited relevant studies, further research is required to develop some effective set-on-demand approaches for 3DPG. To

characterise the structural build-up behaviour, most of the existing studies on 3DPG applied the growth test of static yield stress. SAOS test can provide a better understanding of the early-age structural build-up behaviour [112, 113], while different results can be obtained from the growth test of static yield stress and the SAOS test [93]. Given the importance of structural build-up behaviour for 3DPG, a combination of these two tests would a better choice for the characterisation to understand the underlying mechanism of structural build-up and thus, it could be tailored more effectively during the printing process.

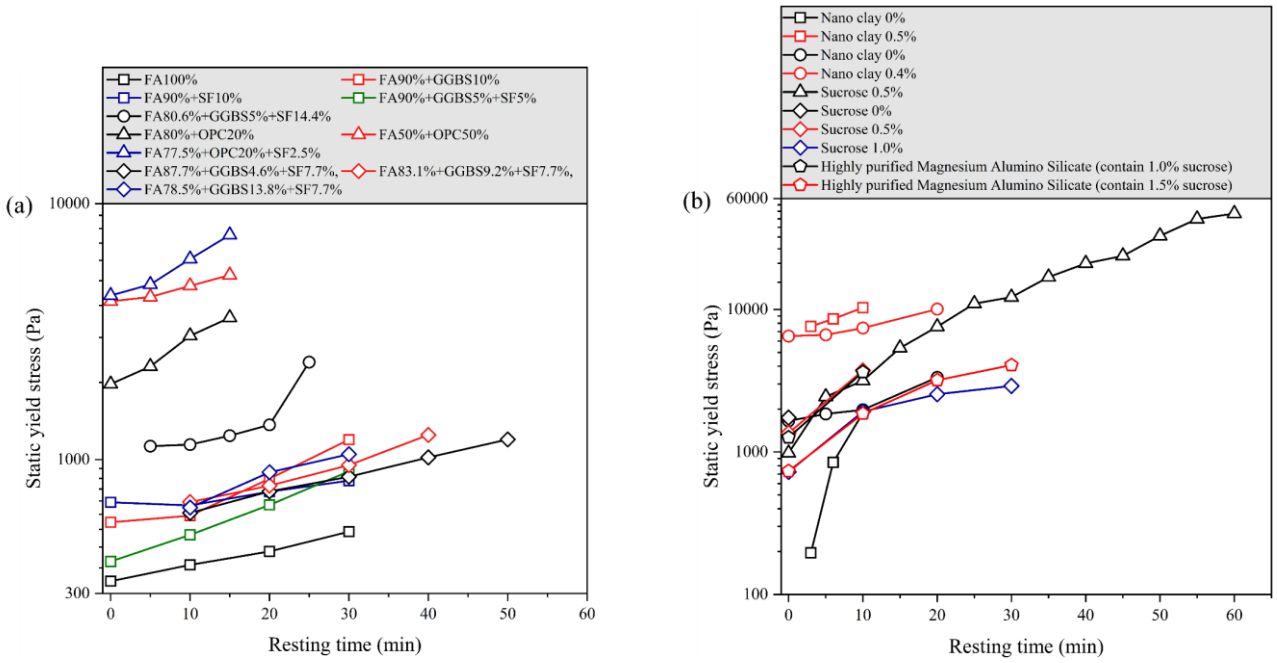

Fig. 11. Evolution of static yield stress: (a) effect of binder type, and (b) effect of additive content (adapted from [14, 15, 34, 35, 52, 54-56]).

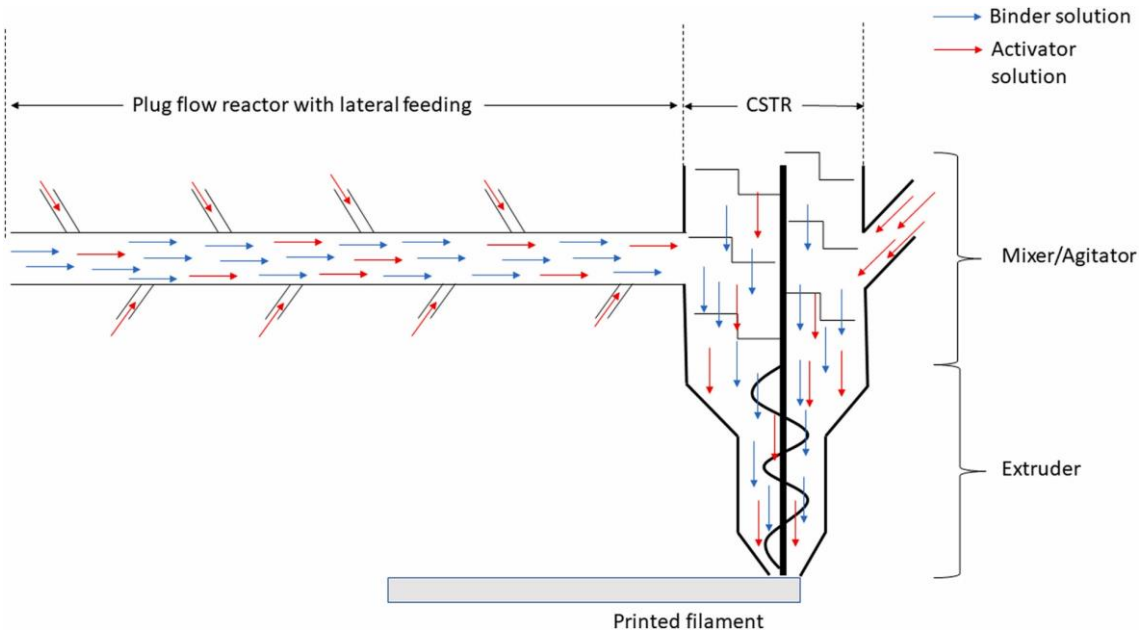

Fig. 12. A proposed print-head design for set-on-demand geopolymers [71].

3.5. Thixotropy and its relation to printability

Thixotropy typifies the reduction of viscosity after subjecting to shear stress while the loss of viscosity recovers following the removal of the applied shear stress [114, 115], which can be characterised using the thixotropy index or viscosity recovery performance. The protocol shown in Fig. 7b can be used to determine the thixotropy index that is calculated as the ratio of the difference between static and dynamic yield stress to dynamic yield stress [53]. On the other hand, the protocol demonstrated in Fig. 7d can give the viscosity recovery ability of test specimens, where different stages during the test are to mimic the delivery and extrusion phases of 3D printing. The higher the thixotropy index or the viscosity recovery ability, the better the thixotropy. The degree of thixotropy can be also estimated with the measured hysteresis loop using the protocol illustrated in Fig. 7c (ramp up and ramp down) [13, 37]. Fig. 13a shows an example of the viscosity recovery test results using the test protocol described in Fig. 7d, and the corresponding viscosity recovery ratio calculated as the ratio of final apparent viscosity to initial apparent viscosity is displayed in Fig. 13b and c.

Guo et al. [37] quantified the thixotropy using the hysteresis area evaluated from the hysteresis loop considering the effects of FA replacements with GGBS and SF. They found that replacing 10% FA with GGBS achieved the highest hysteresis area (higher thixotropy) among other replacements (20% and 30%). Besides, it was observed that using 10% SF to replace FA can increase the hysteresis area of geopolymers by 2.93 times, which can enhance the printability and stacking behaviour of 3DPG [52]. Similar effects were reported for the thixotropic index when the GGBS and SF contents changed [53, 54], as illustrated in Fig. 13b. By contrast, Panda et al. [54] observed that the change of OPC dosage did not exhibit an apparent influence on the thixotropy (Fig. 13b). They also pointed out that because of the improved thixotropy caused by SF, the buildability of printed samples was improved considerably compared to those without SF [54].

Regarding the effect of activator content on the thixotropy of geopolymers, it was found that increasing the activator dosage from 10% to 15% raised the thixotropic index from 1.09 to 1.50, while the further increment to 20% reduced the thixotropic index to 1.27 [53]. This can be ascribed to the plasticising effect of silicates and thus, the bonding between the colloidal particles is weakened. The change in the content of anhydrous Na_2SiO_3 (5-10%) did not lead to a consistent changing trend in the viscosity recovery ratio of geopolymers, which was in the range of 95.9-101.6% [56]. It should be noted that although the mixture activated by 7.5% anhydrous Na_2SiO_3 exhibited a viscosity recovery ratio of 101.6%, the printed structure made from this mixture still failed at the height of 6 layers (see Fig. 9).

As seen in Fig. 13c, the presence of 0.5% nano clay improved the thixotropic index by 1.37 times compared to that without nano clay, owing to the flocculation effect of nano clay particles [52]. The viscosity recovery ratio of geopolymers slightly went up when the nano clay content increased from

0.2% to 0.6% [55], while it almost remained unchanged when 0.5% nano clay was present [52]. It was reported in [56] that the content of sucrose (0.5-1.5%) has an insignificant influence on the viscosity recovery ratio of geopolymers and the incorporation of 0.75% highly purified magnesium aluminium silicate reduced the viscosity recovery ratio of geopolymers by 6.82%, which is inconsistent with the change of static yield stress discussed in Section 3.3.

Muthurkrishnan et al. [56] reported that applying microwave heating can help recover 100% of the initial viscosity for the geopolymers after the extrusion, while geopolymers without microwave heating can only restore up to 25% of the initial viscosity. When microwave heating is used, a network between the reactive particles can be formed to resist the flow or deformation leading to increased viscosity recovery. Besides, implementing the microwave heating at the print-head of the 3D printer can be considered as one of the potential set-on-demand methods for 3DPG [71].

Understanding the thixotropy can only partially reflect the printing performance of investigated mixtures. For instance, conducting the viscosity recovery test can provide information about the buildability of mixtures immediately after extrusion. However, depending on the properties of final printed samples (e.g., shape and height), the real buildability performance can be significantly disparate. Up to now, only a few of the above studies have conducted the buildability tests and correlated the results with thixotropy. The very limited data available in the literature cannot give a clear picture of the intrinsic thixotropic behaviour of geopolymers for 3D printing. Hence, future research is required to investigate the influences of these factors on the thixotropic behaviour and gain a reliable correlation between thixotropy and printability. In addition, other factors (e.g., aggregate and fibre should also be considered.

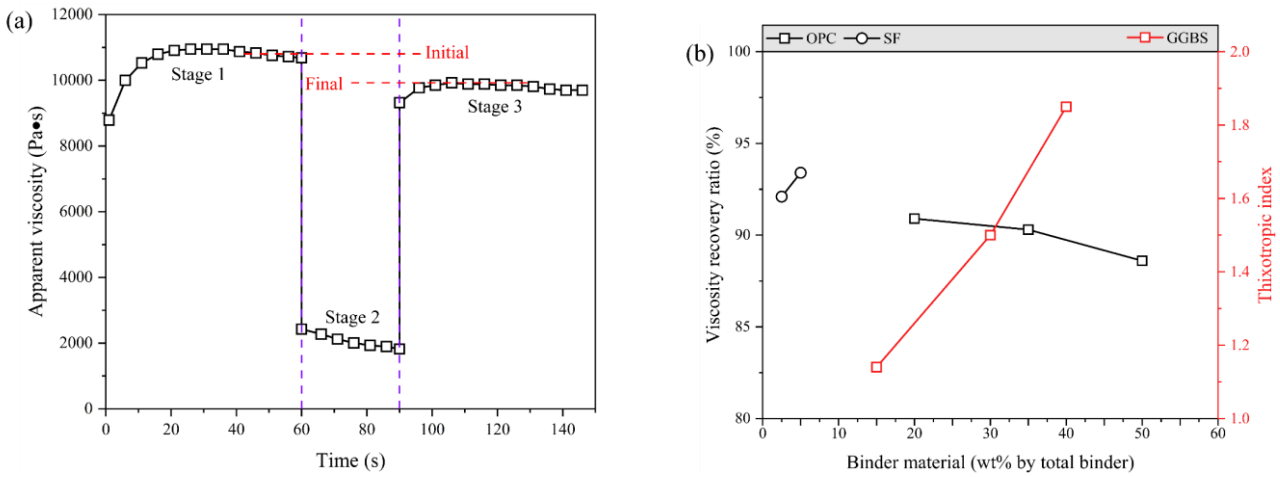

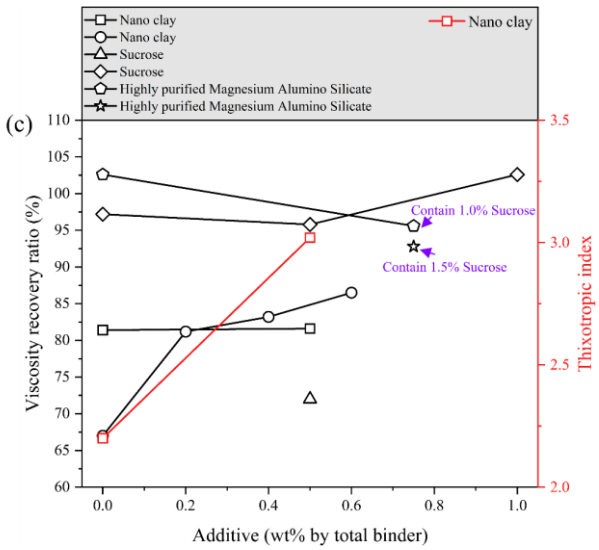

Fig. 13. Viscosity recovery ability and thixotropic index: (a) example of the viscosity recovery test result, (b) effects of binder type and content, and (c) effect of additive content (adapted from [15, 52-56]).

4. Hardened properties of 3D printed geopolymers compared to that of mould-cast geopolymers

4.1. Density

Due to different production techniques, the hardened properties of 3DPG would be different from those of mould-cast geopolymers. A comparison of density of 3DPG and mould-cast geopolymer is presented in Table 3. Regardless of binder type, the density of 3DPG was found to be 4.65-7.89% higher than that of mould-cast geopolymers, which can be attributed to the extra pressure exerted on the samples during the extrusion process [13, 35]. The density of 3DPG would be lower than that of mould-cast geopolymers if the extruded mixtures had a lower flowability and setting time and when the SF contents were 5% and 10%, the density of 3DPG was approximately 2.68-2.87% smaller than that of mould-cast geopolymers [36]. This can be explained by the increased porosity during the extrusion process if the extruded mixture exhibits a short setting time [36]. Thus, the bonding between the layers may be weaker along with more pores between them. Differently, other 3DPG mixtures presented in [36] exhibited a higher density compared to mould-cast geopolymers, which is consistent with that reported in [13, 35].

4.2. Porosity

Given the different fresh properties and extrusion configurations, the porosity inside the printed samples can be either high or low. The porosity of 3DPG in different layers was studied in [43], the results of which are shown in Fig. 14, indicating that the bottom layer had a 1.5-9.73% higher porosity than the top layer. This can be attributed to the potential bleeding issue and non-uniform extrusion pressure, which increased the degree of inhomogeneity inside the printed specimens. This large difference in porosity inside the specimens may lead to variation in mechanical properties along with different loading directions, i.e., anisotropy. Bong et al. [15] also reported that the porosity of 3DPG

was approximately 47.6% higher than that of mould-cast geopolymers owing to the entrapped voids during the layer by layer extrusion [116], which may weaken the mechanical properties. Therefore, to avoid the printing-induced increased porosity, it is crucial to understand the effects of various printing configurations (e.g., printing speed) on the porosity of 3DPG.

4.3. Drying shrinkage

Because of the absence of formwork and the use of aggregates with relatively small sizes, 3D printed concrete is more vulnerable to shrinkage cracking. For geopolymers, the drying shrinkage due to the formation of high capillary pressure between the network of micropores is found to be higher than that of cementitious materials [117], implying that the drying shrinkage issue could be more serious for 3DPG. Thus far, only one study [46] has attempted to reduce the drying shrinkage of 3DPG using sodium carboxymethyl starch, indicating that sodium carboxymethyl starch was effective in reducing the drying shrinkage of geopolymers (Fig. 15). For instance, at 28 d, an approximately 21.92% drop in drying shrinkage can be observed when 8% sodium carboxymethyl starch was present in geopolymers, which can be mainly ascribed to the delayed reaction kinetics, resulting in increased free water content and thus reduced drying shrinkage [46]. Further research on finding more effective measures to mitigate the shrinkage of 3DPG is still required.

Table 3. Comparison of density of 3DPG and mould-cast geopolymers.

Ref.	Binder	Density (kg/m^3)	
		3DPG	Mould-cast geopolymers
[36]	FA70%+GGBS15%+SF15%	2186	2080.6
	FA65%+GGBS20%+SF15%	2210	2064.6
	FA60%+GGBS35%+SF5%	2061	2121.8
	FA60%+GGBS30%+SF10%	2041	2097.4
	FA60%+GGBS25%+SF15%	2275	2113.4
[13]	FA85%+GGBS5%+SF10%	2250	2150
[35]	FA80.6%+GGBS5.0%+SF14.4%	2050	1900

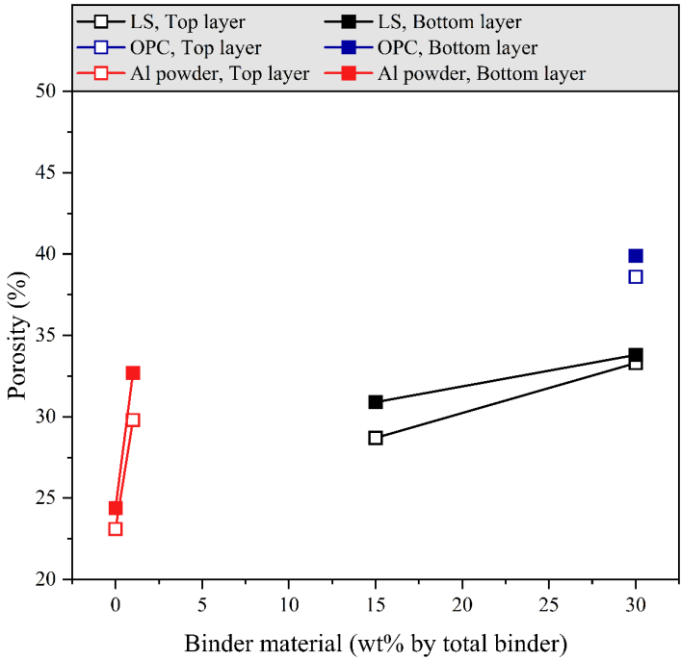

Fig. 14. Porosity of 3DPG in different layers [43].

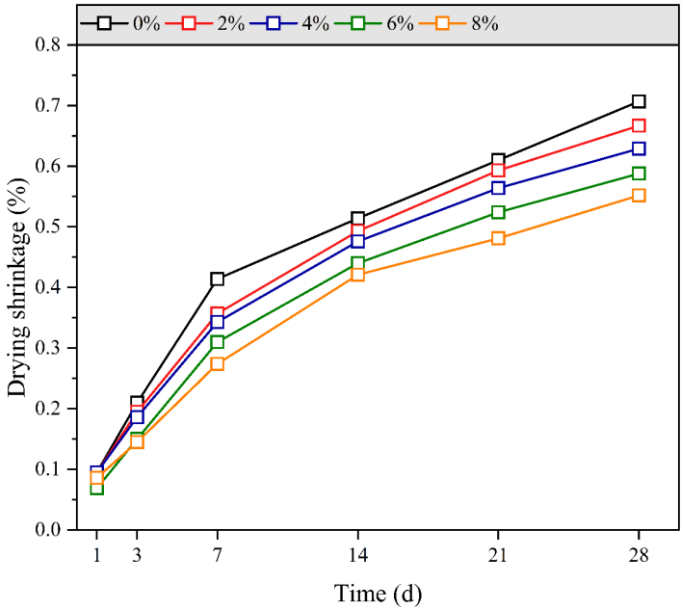

Fig. 15. Effect of sodium carboxymethyl starch content on drying shrinkage of 3DPG [46].

4.4. Compressive strength

Regarding the specimens used for compressive strength tests, most studies listed in Table 1 extracted cubic specimens with various dimensions from the large printed beams. Similar to 3D printed cementitious materials, 3DPG also exhibits an anisotropic performance under compressive loading. Fig. 16a illustrates the loading directions used by existing studies to explore the anisotropic mechanical properties of 3DPG (left image). The measured compressive strength in relation to different variables is presented in Fig. 17, where the symbols of 'x-direction', 'y-direction' and 'z-direction' represent the loading directions parallel, lateral, and perpendicular to the printing direction, respectively.

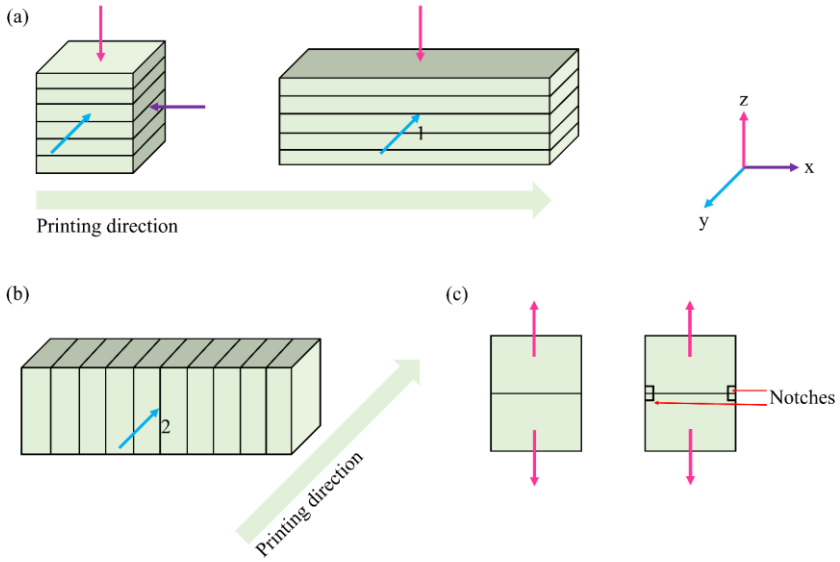

Fig. 16. Loading directions for measuring compressive strength, flexural strength, tensile strength, and tensile bond strength.

Despite meeting the printability requirements, the printed samples should also have acceptable compressive strength for potential engineering applications [21]. Fig. 17a shows the effects of different replacement binder types, curing ages and used loading directions (if the samples are printed) on the compressive strength of geopolymers (3D printed and mould-cast). Regardless of production technique, raising the GGBS content constantly improved the compressive strength of geopolymers because of the increased formation of gels [36, 53]. By contrast, the compressive strength of mould-cast geopolymers showed a consistent decreasing trend when SF was used to replace GGBS, while there did not exist a consistent changing trend regarding the influence of SF for 3DPG [36]. Alghamdi et al. [43] observed that when FA was replaced with LS (15-30%), the compressive strength enhanced but only ranged from 4.2 MPa to 6.5 MPa under a standard curing condition (23 ± 1 ºC and >98% RH), which is not applicable for engineering applications. By changing the curing regime to heat curing at 70 ºC, the compressive strength was increased by up to 221.5% (7.0-20.9 MPa). In addition, the authors found that replacing LS fully with OPC can enhance the compressive strength from 6.5 MPa to 31.2 MPa under standard curing. Besides, the presence of Al powder can help increase the compressive strength of 3DPG by 79.23-193.62%, while this improvement could be primarily associated with the use of Na_2SiO_3 solution (faster dissolution) instead of the addition of Al powder [43].

Fig. 17b illustrates the effect of activator type on the compressive strength of geopolymers, indicating that replacing 50% anhydrous Na_2SiO_3 with GD grade Na_2SiO_3 can achieve an acceptable compressive strength (52.6 MPa) compared to other replacements [15]. Besides, when more Na_2SiO_3 solutions were combined with the NaOH solution, more silicates can be dissolved, resulting in higher reaction rates between particles. Thus, the compressive strength of 3DPG with a higher ratio of

Na_2SiO_3 to NaOH (75:25) was about 19.29-28.70% higher than that with a smaller ratio (60:40) [57]. A similar phenomenon was observed for geopolymers activated by K_2SiO_3 and KOH [57].

Fig. 17c shows the influences of different additives on the compressive strength of geopolymers, which were mostly obtained by conducting the tests on mould-cast geopolymer samples. As discussed earlier, nano clay was useful for improving certain aspects of printability of geopolymers, while it did not benefit the compressive strength. The addition of 0.5% nano clay was found to cause a 27.90% drop in compressive strength compared to the specimens without nano clay [52], which can be ascribed to the increased porosity induced by the poor dispersion of nano clay particles [49]. Similar effects on compressive strength were reported when sucrose and sodium carboxymethyl starch were present [15, 46]. By contrast, because of the crack bridging behaviour, it was reported that utilising 0.1% nano-graphite platelet can improve the compressive strength by 17.8% but further addition weakened the compressive strength [36, 118].

Fig. 17d presents the anisotropic compressive behaviour of 3D printed glass fibre reinforced geopolymer composites. Regardless of loading direction, glass fibres had a negative influence on compressive strength. It can be seen from Fig. 17 d that the incorporation of 1.0% glass fibre led to a 10.96-16.92% lower compressive strength than that with 0.25% glass fibre [40], which can be attributed to the poor fibre orientation caused by the extrusion, resulting in more voids around the fibres. Li et al. [42] studied the effect of printing path on the compressive strength of 3DPG reinforced with steel cables and the results along with the used printing paths are depicted in Fig. 17e. It can be observed that applying path B to print the geopolymer composites can achieve the highest strength of around 41.5 MPa. Besides, the ductility and energy absorption ability of geopolymers under compressive loading can be improved by adding steel cables. For instance, as displayed in Fig. 18, without the cable reinforcement, the specimen was damaged significantly with oblique cracks, while the specimens reinforced with steel cables remained the original cubic shape [42].

Some studies [15, 36] found that the compressive strength of mould-cast geopolymers was higher than that of 3DPG due to the increased porosity between the layers for 3DPG, while depending on the 3D printing process, the compressive strength of 3DPG could be either higher or lower as compared with mould-cast geopolymers [13]. Regarding the anisotropic behaviour, the compressive strength of 3DPG in x-direction was generally 2.35-23.04% higher than that in y- and z-direction [13, 15, 40], which can be attributed to the better compaction in x-direction because of the high pressure induced by the extrusion [15]. Applying the load in x-direction can lead to a more uniform stress distribution while the layers started to slip from each other when the load was imposed in y-direction [13]. Besides, the bonding strength between the layers plays a critical role in the anisotropic behaviour of 3DPG, which can be influenced by both fresh properties (especially structural build-up) of geopolymers and printing configurations (especially printing layer cycle time) of 3D printing. As

mentioned in Section 3.4, if the materials process a stable structural build-up behaviour, the risk of encountering pumping and extrusion problems may be reduced. A stable structural build-up may also provide sufficient time for the layers to bond. However, different construction rates of printed objects may require different rates of structural build-up for the materials. It could be assumed that the printing speed should be quick enough if the material has a higher structural build-up to avoid any bonding problems, while the printing speed should be slow if the material has a slower structural build-up to ensure a sufficient yield strength can be achieved for the deposited layer. As illustrated in Fig. 19, if the bond between layers is not well, there may exist large voids, leading to an increased heterogeneity and thereby, the compressive strength would be lower. As the 3D printing process can affect the compressive strength of 3DPG, the effect of printing layer cycle time was studied and reported in [58], indicating that there was no significant influence on compressive strength when the printing layer cycle time was changed from 2 min to 15 min.

Unlike mould-cast geopolymers, the compressive strength of 3DPG can be strongly affected by the production process, e.g., extrusion. Moreover, a significant variation in compressive strength can be observed when different loading directions are applied, which may hinder the wide application of 3DPG. To improve the compressive strength of printed samples while avoiding the considerable anisotropic behaviour, the effect of various printing configurations on the compressive strength needs to be estimated, which has been rarely explored to date. A better 3D printing production of geopolymers can be achieved by selecting suitable printing configurations. Besides, the analysis of the material's structural build-up behaviour should be included during the optimisation of 3D printing configurations. Special attention should be paid to the 3DPG reinforced with short fibres as the fibre orientation can be affected by the 3D printing process as well. Lastly, it is essential to find a balance between printability and compressive strength of 3DPG as the incorporation of some additives can significantly improve its printability but weakens the compressive strength.

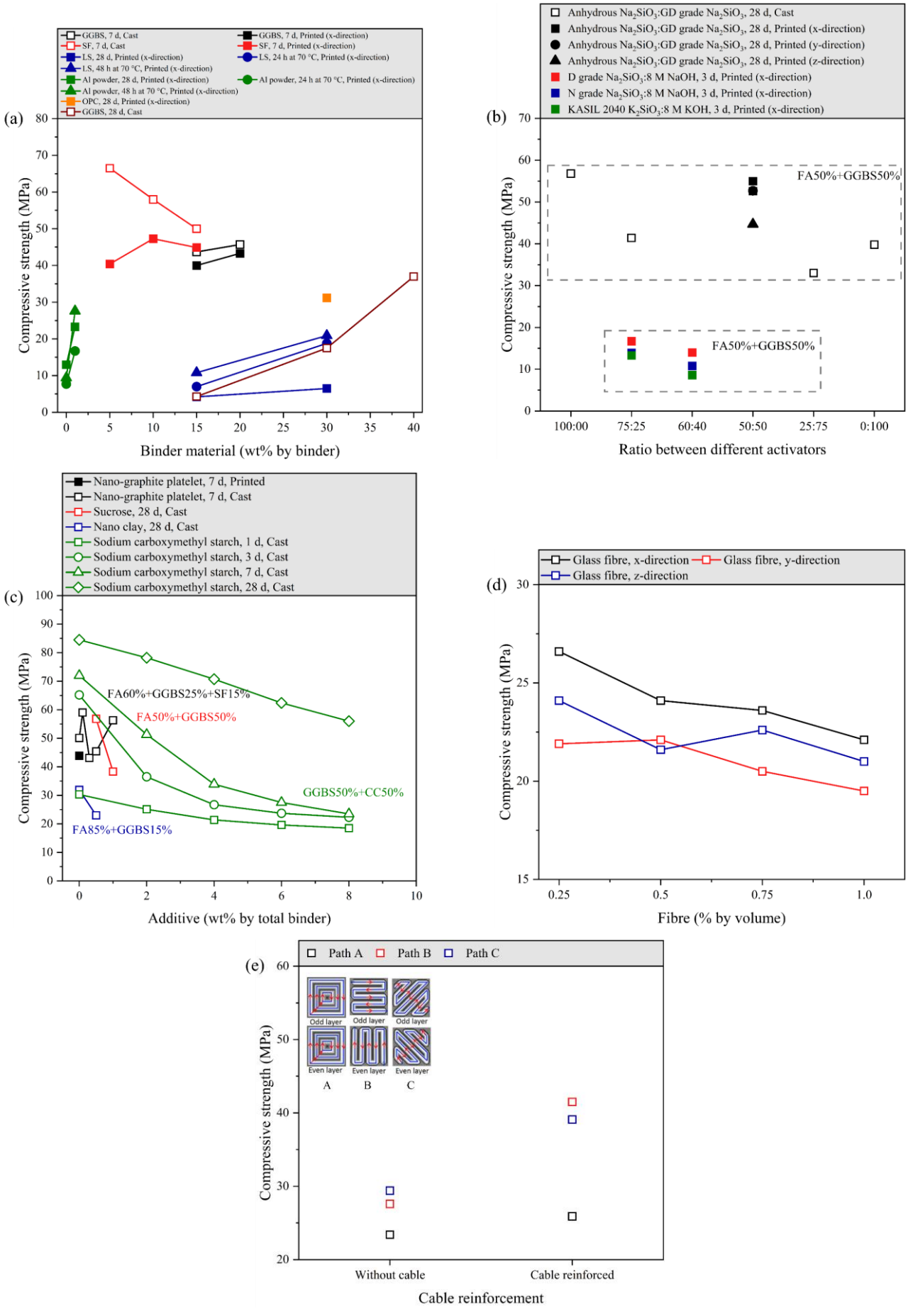
(a)
GGBS, 7 d, Cast
SF, 7 d, Cast
LS, 28 d, Printed (x-direction)
LS, 48 h at 70 °C, Printed (x-direction)
Al powder, 28 d, Printed (x-direction)
Al powder, 48 h at 70 °C, Printed (x-direction)
OPC, 28 d, Printed (x-direction)
GGBS, 28 d, Cast
GGBS, 7 d, Printed (x-direction)
SF, 7 d, Printed (x-direction)
LS, 24 h at 70 °C, Printed (x-direction)
Al powder, 24 h at 70 °C, Printed (x-direction)
Compressive strength (MPa)
Binder material (wt% by binder)
(b)
Anhydrous Na2SiO3:GD grade Na2SiO3, 28 d, Cast
Anhydrous Na2SiO3:GD grade Na2SiO3, 28 d, Printed (x-direction)
Anhydrous Na2SiO3:GD grade Na2SiO3, 28 d, Printed (y-direction)
Anhydrous Na2SiO3:GD grade Na2SiO3, 28 d, Printed (z-direction)
D grade Na2SiO3:8 M NaOH, 3 d, Printed (x-direction)
N grade Na2SiO3:8 M NaOH, 3 d, Printed (x-direction)
KASIL 2040 K2SiO3:8 M KOH, 3 d, Printed (x-direction)
FA50%+GGBS50%
FA50%+GGBS50%
Compressive strength (MPa)
100:00
75:25
60:40
50:50
25:75
0:100
Ratio between different activators
(c)
Nano-graphite platelet, 7 d, Printed
Nano-graphite platelet, 7 d, Cast
Sucrose, 28 d, Cast
Nano clay, 28 d, Cast
Sodium carboxymethyl starch, 1 d, Cast
Sodium carboxymethyl starch, 3 d, Cast
Sodium carboxymethyl starch, 7 d, Cast
Sodium carboxymethyl starch, 28 d, Cast
FA60%+GGBS25%+SF15%
FA50%+GGBS50%
GGBS50%+CC50%
FA85%+GGBS15%
Compressive strength (MPa)
Additive (wt% by total binder)
(d)
Glass fibre, x-direction
Glass fibre, y-direction
Glass fibre, z-direction
Compressive strength (MPa)
Fibre (% by volume)
(e)
Path A
Path B
Path C
Odd layer
Even layer
A
B
C
Compressive strength (MPa)
Without cable
Cable reinforced
Cable reinforcement

Fig. 17. Compressive strength of 3DPG: (a) effects of binder type and content, (b) effect of activator type, (c) effect of additive content, (d) effects of glass fibre content and loading direction, and (e) effects of printing path and steel cable reinforcement (adapted from [15, 36, 40, 42, 43, 46, 52, 53, 57]).

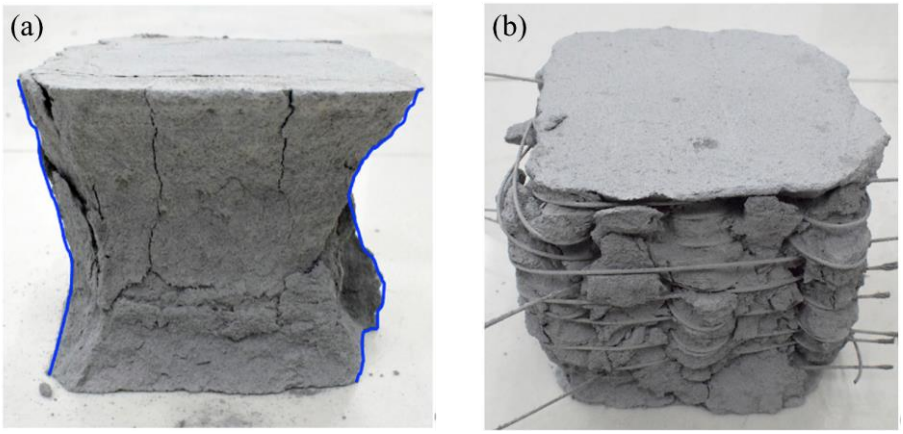

Fig. 18. Compressive failure pattern: (a) without cable reinforcement and (b) with cable reinforcement [42].

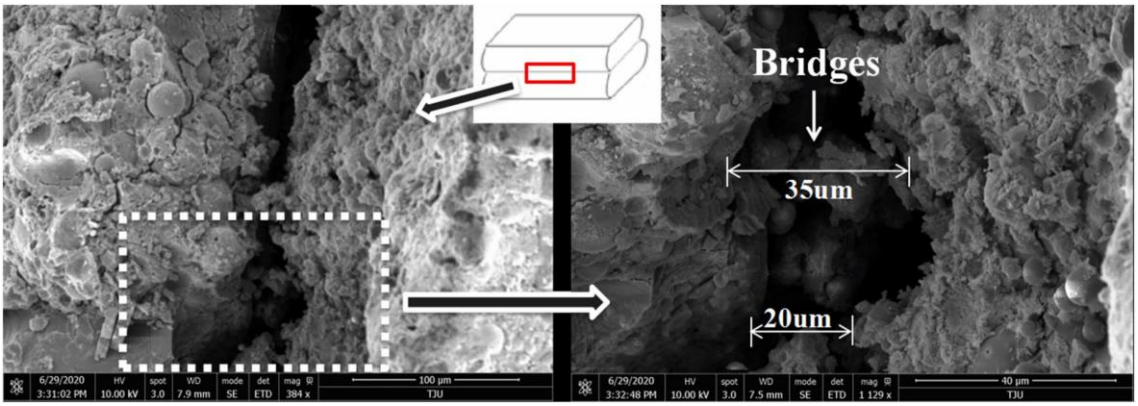

Fig. 19. Microstructure of 3DPG [37].

4.5. Flexural strength and ductility

Three different loading directions (Fig. 16a and b) were used to characterise the flexural strength of 3DPG, the results of which are presented in Fig. 20. Regarding the relevant notations, 'y1-direction', 'y2-direction' and 'z-direction' represent the loading direction lateral, parallel, and perpendicular to the printing direction, respectively. Similar to that of compressive strength, it was found that increasing either LS or Al powder dosage improved the flexural strength of 3DPG by 2.38%-145.45% under various curing regimes (Fig. 20a) [43]. It is worth noting that although replacing LS with OPC can enhance the compressive strength (Fig. 17a), the flexural strength was about 52.38% lower when the OPC was present due to the lower interfacial strength [43]. As seen in Fig. 20a, the flexural strength of mould-cast geopolymers increased with the increase of GGBS content, while the flexural strength of 3DPG reduced with the increasing GGBS dosage, which can be ascribed to the poor microstructure and weak bond between each layer of 3DPG [36]. Similarly, different changing trends

were observed for the flexural strength of 3DPG and mould-cast geopolymers against SF content [36]. Thus, more tests are required to confirm these findings.

Consistent with the results of compressive strength (Fig. 17c), Fig. 20b indicates a decreasing trend in flexural strength at different curing ages when the sodium carboxymethyl starch was added with a more apparent reduction at 28 d [46]. As mentioned earlier, nano-graphite platelet can effectively inhibit and bridge the cracks during the loading and hence, the flexural strength of geopolymers was improved by 47.1% after incorporating 1.0% nano-graphite platelet, as reported by [36]. However, it is necessary to verify these improvements by testing 3DPG samples.

Fig. 20c presents the effects of glass fibre content and length on the flexural strength of 3DPG, where 'L3', 'L6', and 'L8' denote the length of glass fibre, i.e., 3 mm, 6 mm and 8 mm. Different from compressive strength, it can be seen from Fig. 20c that the flexural strength of 3DPG is generally enhanced with the increasing glass fibre dosage and glass fibre length [40], which can be ascribed to the fibre bridging effect [63]. Ma et al. [41] explored the effects of printing paths and steel cable reinforcement on the flexural strength of 3DPG, the results of which are demonstrated in Fig. 20d. It should be noted that the printing paths they adopted were the same as those shown in Fig. 17e. The authors revealed that reinforcing 3DPG with steel cables exhibited a higher flexural strength as compared with plain 3DPG, and combing path C and steel cable reinforcement can achieve a flexural strength of about 28.5 MPa for 3DPG composites (Fig. 20d). Similar positive effects of using steel cables were reported by Lim et al. [39], who investigated the effect of steel cable diameter on the flexural strength of 3DPG. The results are also summarised in Fig. 20d, where 'D1', 'D1.5', and 'D2' represent that the diameter of the used steel cable is 1 mm, 1.5 mm and 2 mm, respectively. It is indicated that increasing the diameter of steel cable can lead to a consistently increasing trend in flexural strength of 3DPG. Given the better fibre bridging behaviour, Al-Qutaifi et al. [47] pointed out that the geopolymer mixtures containing 1.0% steel fibre can outperform the mixtures reinforced with 0.5% PP fibre, regardless of loading direction (Fig. 20e).

Chougan et al. [36] suggested that the flexural strength of most investigated 3DPG mixtures was lower than that of mould-cast geopolymers due to the weak bonding condition between layers. For instance, the flexural strength of mould-cast geopolymer containing 5% SF was about 38.3% higher than that of 3DPG (Fig. 20a). However, a conclusion cannot be drawn based on just one relevant study. Like compressive strength, the flexural strength of 3DPG also exhibits anisotropic behaviour. As mentioned in Section 4.4, when fibres are not included, the bonding strength between layers is the key factor to cause the anisotropic behaviour, which can be influenced by the fresh properties of materials and printing configurations. However, the anisotropic behaviour can be quite distinct when fibres are added as the fibre orientation would be affected by 3D printing [60]. The flexural strength of a printed element can be even higher than that of a mould-cast specimen if the maximum bending

stress is induced at the bulk material rather than the interface [2]. As reported in [58] that the flexural strength of 3DPG in z-direction was about 51.43-64.86% higher than that in y1-direction, which can be attributed to the induced location of the maximum bending stress. Similarly, for 3DPG composites, the flexural strength in z-direction was found to be higher than those in y1- and y2-direction when the length of glass fibre was 8 mm as the fibres were mostly orientated perpendicular to the loading direction, resulting in better crack-bridging behaviour [40]. The weak bond between layers in y1- and y2-direction may lead to flexural failure before the action of fibres. However, the higher flexural strength in z-direction did not exist when the length of glass fibres was 3 mm and 6 mm (Fig. 20c). Al-Qutaifi et al. [47] demonstrated that the flexural strength of plain geopolymers and geopolymer composites with 0.5% PP fibre in y1-direction was higher than that in z-direction (Fig. 20e), where the geopolymers were cast into the mould layer by layer rather than 3D printing. Thus, the bonding and fibre orientation could be considerably different. As discussed earlier, printing layer cycle time can significantly affect the bond strength of 3DPG and therefore, its effect on the flexural strength is also summarised in Fig. 20e. The flexural strength reduced with the increase of printing layer cycle time, suggesting the importance of the bonding between each layer [47, 58]. Moreover, the number of printing layer can affect the flexural behaviour of 3DPG composites containing 2.0% PVA fibre [51]. As seen in Fig. 21, the specimen with only one printing layer seems to have a better flexural strength as the inter-layer bonding strength does not exist for one layer printing. Nevertheless, two curves with large deviations are not adequate to conclude this effect. Although several studies have attempted to understand the anisotropic behaviour of the flexural strength of 3DPG, a clear conclusion is difficult to be made given the different trends and limited database. Therefore, it is vital to systematically investigate the effects of various printing configurations on the anisotropic behaviour, especially when fibres are incorporated. In addition, the fibre bridging behaviour crossing the layer has still not been investigated, which may play an essential role in the flexural behaviour. Furthermore, other fibre types such as hybrid fibre reinforcement (e.g., hybrid steel and PP fibres) can be considered to better improve the flexural strength of 3DPG.

Typically, the flexural deflection at the highest applied load or the end of loading can be used to indirectly reflect the ductility behaviour. Fig. 22a shows the effects of glass fibre content and length at various loading directions on the flexural deflection of 3DPG composites, where the notations in the legend are consistent with those in Fig. 20c. It can be found that except for y1-direction, the flexural deflection of 3DPG composites was improved as the glass fibre content increased [40]. For instance, with the increase of glass fibre content from 0.25% to 1.0%, the flexural ductility in z-direction was increased by 16.67-135.29%, which can be ascribed to the fibre-matrix interaction after crack initiation [63]. There would be more effective fibres with the increasing fibre content, which can resist the crack propagation [119]. The bridging fibres would experience slippage/sliding during

the fibre pull-out and thus the ductility of the whole composites would be enhanced [120]. As seen in Fig. 22a, the influence of glass fibre length was less sensitive as compared with the effect of glass fibre content [40]. For instance, only the flexural deflection of 3DPG composites was increased with the increasing glass fibre length when the fibre content was 0.25% with loading in z-direction. In y1-direction, some negative influences (a reduction of 8-30%) can even be observed with the change of fibre length. Similar to flexural strength, the flexural deflection of 3DPG composites with glass fibres in y1-direction was lower compared to those in other directions [40]. Therefore, as mentioned earlier, if the bonding between layers is not well, the contribution of fibres to the flexural behaviour of 3DPG would be diminished, which suggests the importance of assessing the fibre condition across the layers. Fig. 22b depicts the effects of printing path and steel cable diameter on the flexural deflection of 3DPG composites (notations in the legend are consistent with those in Fig. 20d), which indicates that the flexural deflection can be improved the most when path C was used to print the samples [41]. Besides, increasing the steel cable diameter led to increased flexural deflection for 3DPG composites [39]. These results are consistent with the findings for flexural strength. The failure patterns shown in Fig. 22c and d can prove that utilising steel cables can transform the brittle behaviour of 3DPG into the ductile behaviour along with multiple micro-cracks [41].

Overall, very limited experimental data are available on the ductility of 3DPG composites, while flexural deflection is an indirect parameter for characterising ductility. Conducting uniaxial tension tests to monitor the strain changes during the tensile loadings can better characterise the ductility of 3DPG, which is discussed in detail below.

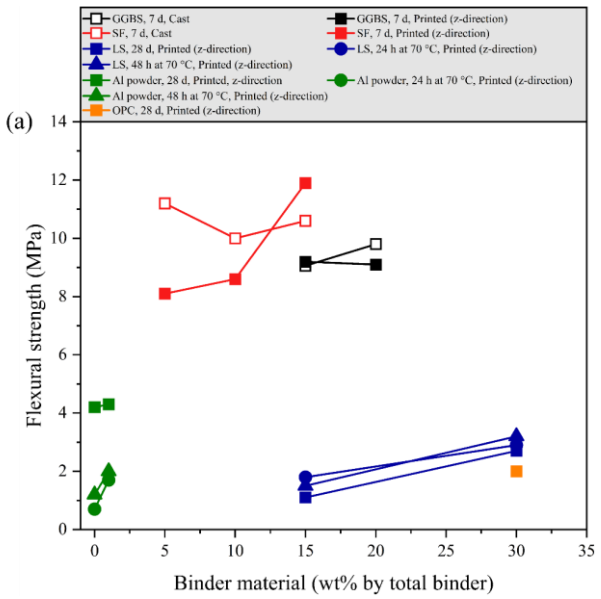
(a)
GGBS, 7 d, Cast
GGBS, 7 d, Printed (z-direction)
SF, 7 d, Cast
SF, 7 d, Printed (z-direction)
LS, 28 d, Printed (z-direction)
LS, 24 h at 70 °C, Printed (z-direction)
LS, 48 h at 70 °C, Printed (z-direction)
Al powder, 28 d, Printed, z-direction
Al powder, 24 h at 70 °C, Printed (z-direction)
Al powder, 48 h at 70 °C, Printed (z-direction)
OPC, 28 d, Printed (z-direction)
Flexural strength (MPa)
Binder material (wt% by total binder)

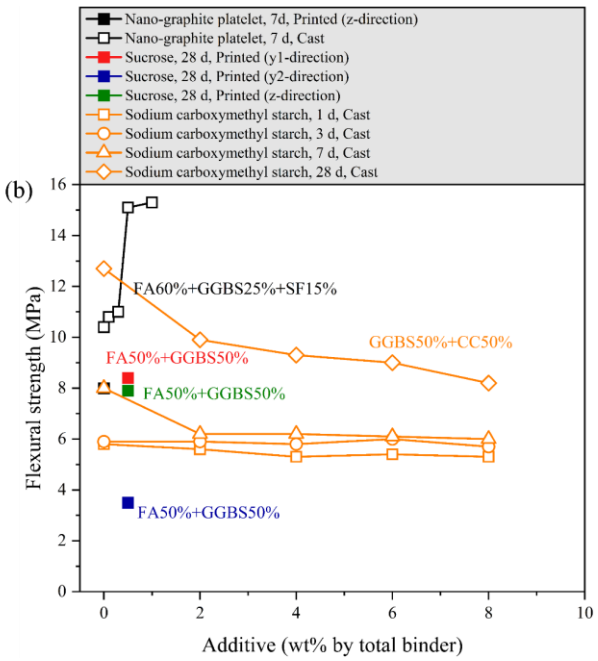
(b)
Nano-graphite platelet, 7d, Printed (z-direction)
Nano-graphite platelet, 7 d, Cast
Sucrose, 28 d, Printed (y1-direction)
Sucrose, 28 d, Printed (y2-direction)
Sucrose, 28 d, Printed (z-direction)
Sodium carboxymethyl starch, 1 d, Cast
Sodium carboxymethyl starch, 3 d, Cast
Sodium carboxymethyl starch, 7 d, Cast
Sodium carboxymethyl starch, 28 d, Cast
FA60%+GGBS25%+SF15%
GGBS50%+CC50%
FA50%+GGBS50%
FA50%+GGBS50%
FA50%+GGBS50%
Flexural strength (MPa)
Additive (wt% by total binder)

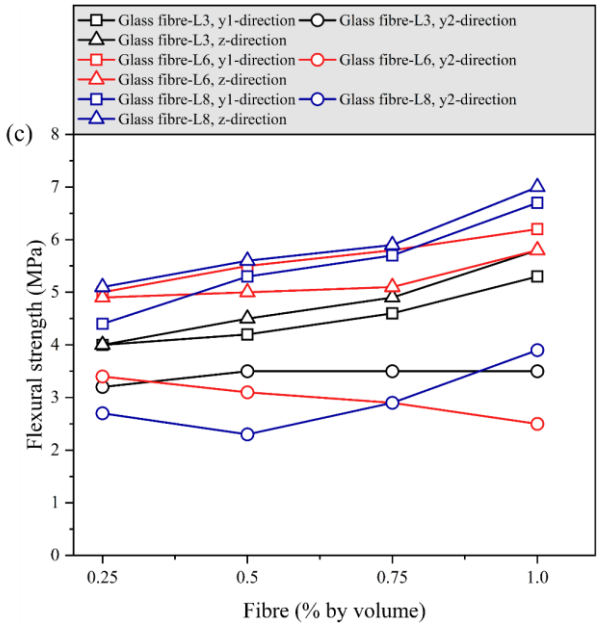
(c)
Glass fibre-L3, y1-direction
Glass fibre-L3, y2-direction
Glass fibre-L3, z-direction
Glass fibre-L6, y1-direction
Glass fibre-L6, y2-direction
Glass fibre-L6, z-direction
Glass fibre-L8, y1-direction
Glass fibre-L8, y2-direction
Glass fibre-L8, z-direction
Flexural strength (MPa)
Fibre (% by volume)

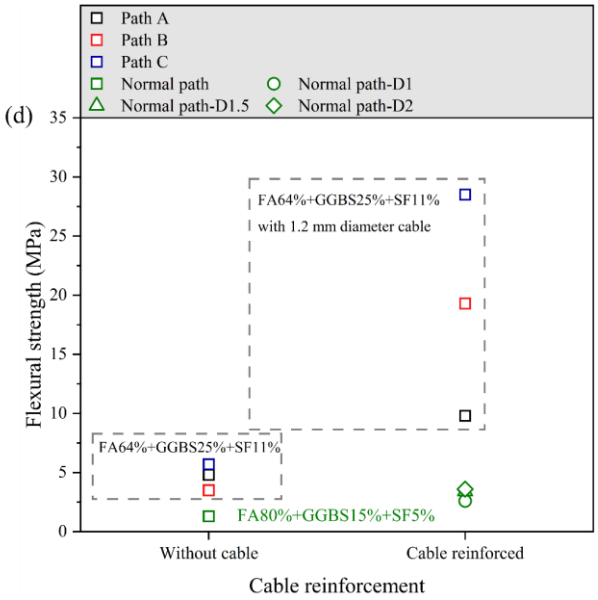
(d)
Path A
Path B
Path C
Normal path
Normal path-D1
Normal path-D1.5
Normal path-D2
FA64%+GGBS25%+SF11%
with 1.2 mm diameter cable
FA64%+GGBS25%+SF11%
FA80%+GGBS15%+SF5%
Flexural strength (MPa)
Without cable
Cable reinforced
Cable reinforcement

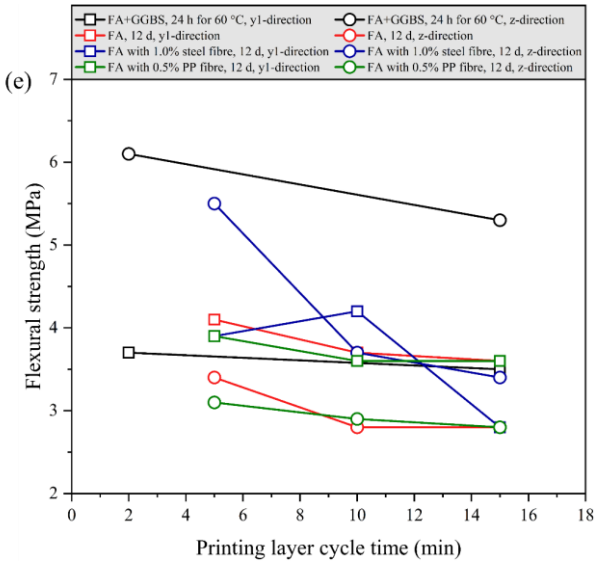
(e)
FA+GGBS, 24 h for 60 °C, y1-direction
FA+GGBS, 24 h for 60 °C, z-direction
FA, 12 d, y1-direction
FA, 12 d, z-direction
FA with 1.0% steel fibre, 12 d, y1-direction
FA with 1.0% steel fibre, 12 d, z-direction
FA with 0.5% PP fibre, 12 d, y1-direction
FA with 0.5% PP fibre, 12 d, z-direction
Flexural strength (MPa)
Printing layer cycle time (min)

Fig. 20. Flexural strength of 3DPG: (a) effects of binder type and content, (b) effect of additive content, (c) effects of glass fibre content, glass fibre length and loading direction, (d) effects of printing path and steel cable diameter, and (e) effect of printing layer cycle time (adapted from [15, 36, 39-41, 43, 46, 47, 58]).

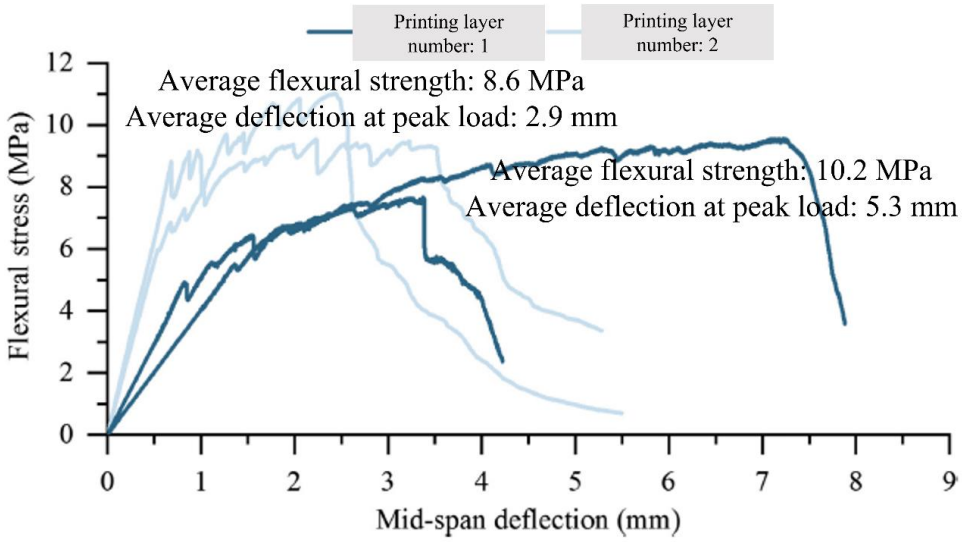

Fig. 21. Effect of printing layer number on flexural behaviour of 3DPG composites [51].

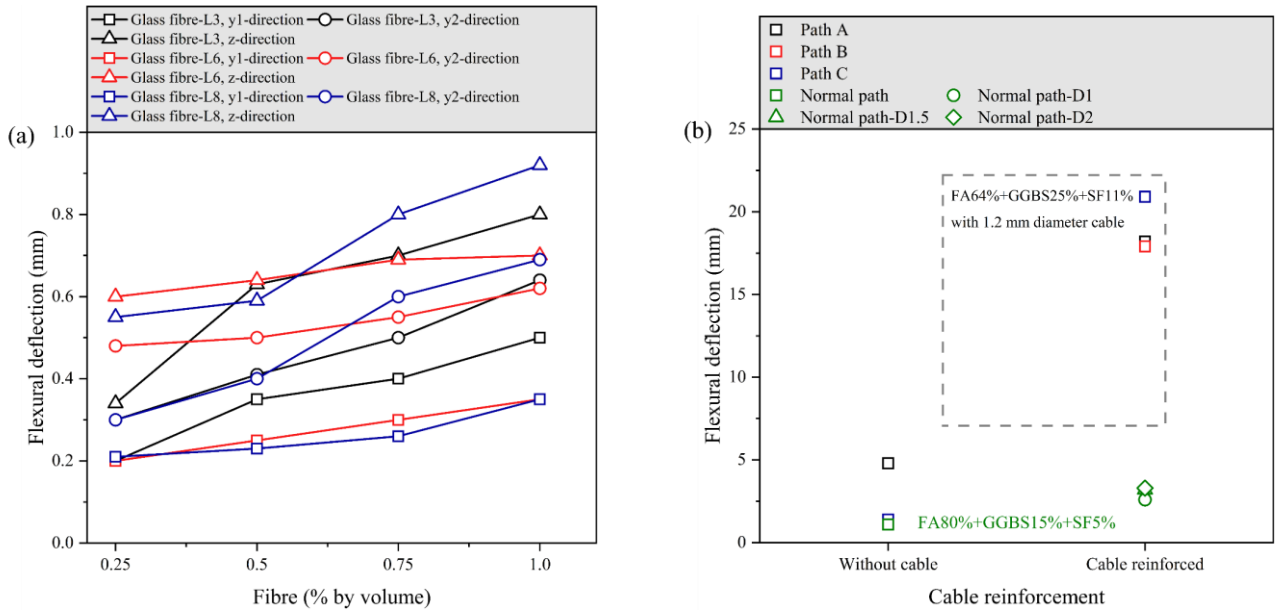

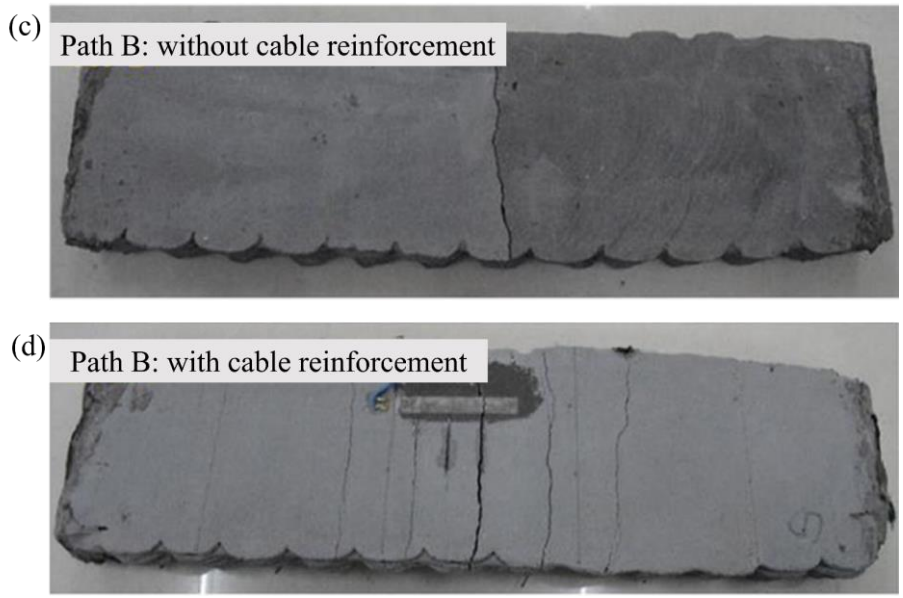

Fig. 22. Flexural deflection of 3DPG: (a) effects of glass fibre content, glass fibre length and loading direction, (b) effects of printing path and steel cable diameter, and flexural failure patterns of samples with (c) and without (d) cable reinforcement [39-41].

4.7. Tensile strength

Fig. 23 demonstrates the tensile strength and tensile strain capacity of 3DPG composites. As observed from Fig. 23a, irrespective of loading direction, with the increase of glass fibre content from 0.25% to 1.0%, the tensile strength of 3DPG composites was enhanced by 81-96.1% [40]. When the loading was parallel to the printing direction, the tensile strength of 3DPG was higher as compared with the loading direction perpendicular to the printing direction. As mentioned previously, most fibres are ideally aligned along the printing direction and thus, the cracks induced by the tensile loading can be resisted and bridged by the fibres. Contrarily, the tensile strength would be affected by the bonding condition between each layer if the loading perpendicular to the printing direction is applied. The fibre crossing the layer is a concern, which has not been studied [40]. The used printing paths shown in Fig. 23b are consistent with those in Fig. 17e. It shows that different from the compressive strength and flexural strength, when using path A or path B as the printing path, the tensile strength can be improved and applying path A to print the geopolymer composites can achieve the highest tensile strength of 4.7 MPa [42]. Plain 3DPG without any reinforcing materials is very brittle with a tensile strain of only 0.03%-0.05%. By contrast, incorporating the steel cables can strongly enhance the tensile strain of 3DPG by 22.2-46.3 times. It is interesting to note that the tensile strength was more sensitive to the applied printing path as it can result in different fibre orientations. As seen in Fig. 23c, the steel cable was pulled out when it was oriented perpendicular to the loading direction, which would improve the ductility of the whole composites [42]. By contrast, the authors observed a broken steel cable when it was parallel to the loading direction along with several parallel flaws.

Although the above results showed certain improvements when glass fibres or steel cables are incorporated, corrosions or fractures of these fibres may happen under highly alkaline environments. These may affect the long-term behaviour of these 3DPG composites if used for engineering applications. To avoid these issues while improving the tensile behaviour, polymeric fibres such as PVA or polyethylene fibres can be used for developing 3D printed strain hardening geopolymer composites. So far, strain hardening cementitious composites have been successfully developed for 3D printing applications [121-123], while no comprehensive research is found for geopolymers.

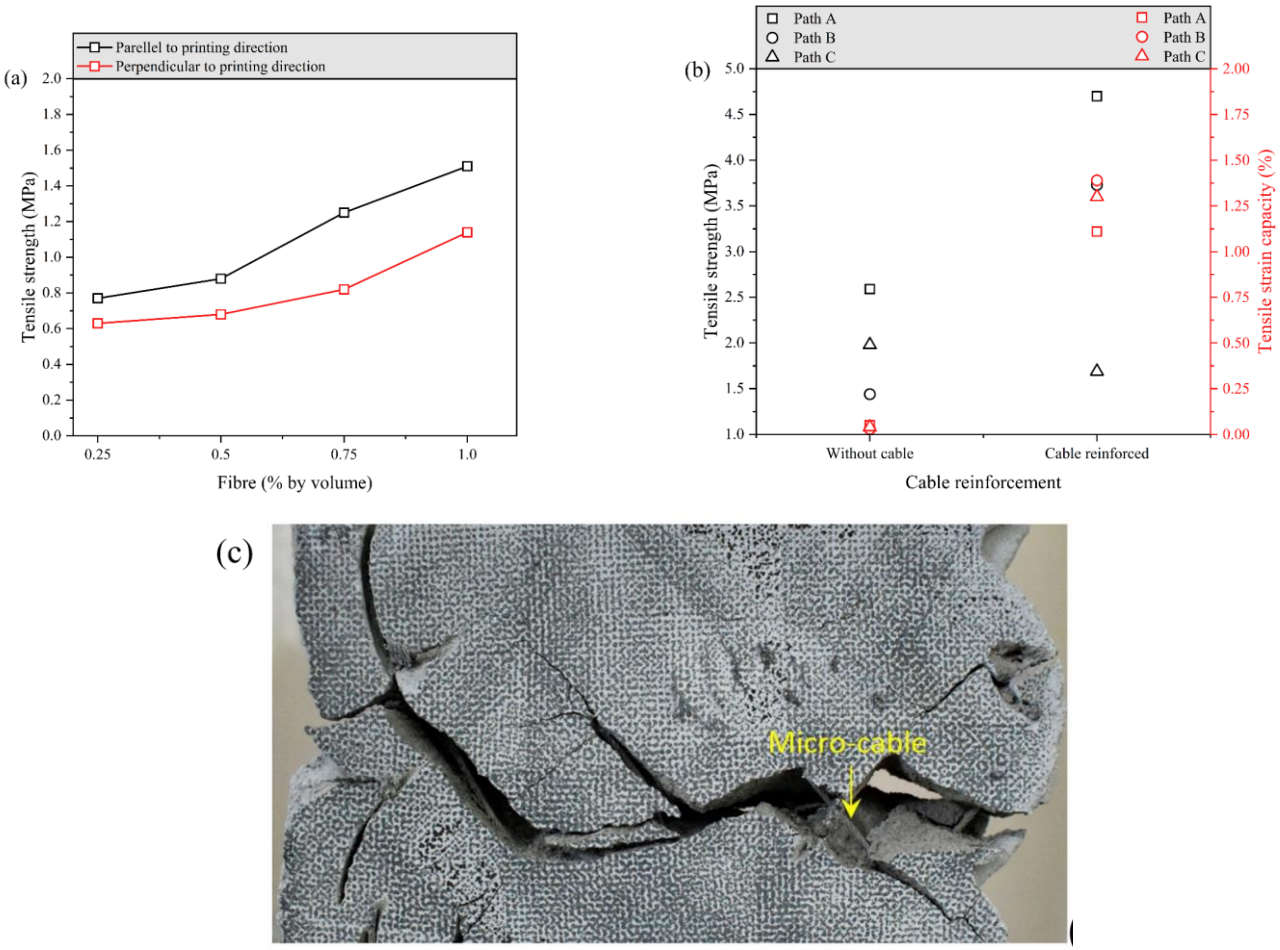

Fig. 23. Tensile strength of 3DPG composites: (a) effects of glass fibre content and loading direction, (b) effects of printing path and steel cable reinforcement, and (c) an image showing the cracking interface [40, 42].

4.8. Bond strength

Bond strength plays a critical role in the hardened properties for 3D printed concrete, which is usually determined using the testing protocols shown in Fig. 16c. Panda et al. [38] investigated the effect of different activator moduli (1.6-2.0) on the tensile bond strength of 3DPG and found that it tended to be higher when the activator with a higher modulus was used, mainly due to a slower increase rate of structural build-up. They found that the bonding surface for 3DPG with an activator modulus of 2.0 had a higher roughness as compared with the 3DPG with an activator modulus of 1.6. As reported in [50], applying microwave heating can improve the viscosity recovery ability and thereby, enhancing

the buildability and bond strength at both 7 d and 28 d of 3DPG. For instance, an 87.5% rise in bond strength of 3DPG composites was found after microwave heating of 10 s, while the bond strength reduced if the heating lasted over 10 s due to the fast hardening rate. Therefore, it is crucial to find a suitable microwave heating time.

As aforementioned, the printing configurations can also considerably impact the bond strength of 3DPG. Fig. 24 depicts the effects of different printing configurations including printing layer cycle time, printing speed and nozzle standoff distance on the tensile bond strength of 3DPG. As expected, the tensile bond strength showed a reducing trend when the printing layer cycle time increased [13, 35, 58]. For instance, the tensile bond strength of 3DPG was declined by about 76.4% when the printing layer cycle time changed from 0 min to 20 min [13]. With the increase of printing layer cycle time, the stiffening condition of the deposited layer would be difficult to bond with the upcoming extruded layer, resulting in reduced bond strength. Besides, increasing the printing speed and nozzle standoff distance also negatively affect the bond strength and thus, these parameters need to be carefully selected [35]. All these suggest the importance of controlling printing configurations as the use of inappropriate printing parameters could significantly weaken the bond strength, leading to poor mechanical properties and durability. As mentioned in Section 4.4, the material's structural build-up should be included during the optimisation of printing configurations, as for different structural build-up behaviours, the optimal printing configurations could alter. To this end, more comprehensive evaluations are still needed to obtain a solid conclusion for the optimal printing configurations in terms of the bond strength. Besides, more other factors such as binder types and fibre types should be considered.

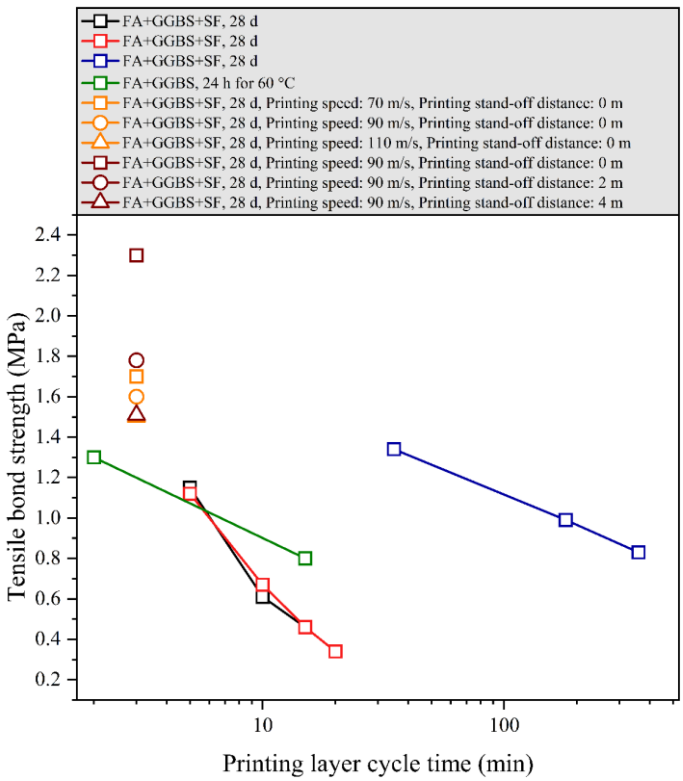

Fig. 24. Effects of printing configurations (printing layer cycle time, printing speed, nozzle standoff distance) on tensile bond strength of 3DPG [13, 35, 58].

5. Sustainability

The embodied carbon and embodied energy are normally used for sustainability assessment since the other parameters (e.g., cost) can vary with time and location [21, 119, 124]. Besides, the most relevant system boundary for 3D printing technology would be cradle-to-gate [21]. Hence, to assess the sustainability of 3DPG, the environmental impacts (embodied carbon and embodied energy) in the cradle-to-gate phase (all processes before the production of 3DPG) are considered. Two optimal 3DPG mix proportions presented in [15, 34] were chosen for the sustainability analysis here while other relevant studies from 3D cementitious materials [125, 126] were also considered for comparison. Depending on the mix compositions, their embodied carbon and embodied energy can be calculated using the life cycle inventory data in Table 4, which were mainly collected from the literature [124, 127-132]. The functional indicators (typically, compressive strength or durability-related property) need to be considered for sustainability analysis [21, 133-135]. As the initial static yield stress can significantly affect the printability of 3DPG, it was also included as one of the functional indicators here in addition to the compressive strength. The results of sustainability assessment are presented in Table 5 and Fig. 25.

As seen in Table 5, the mixture containing 80% OPC and 20% FA exhibited the highest embodied carbon and embodied energy of 555.51 kg CO2.eq/m^3 and 3173.6 MJ/m^3, respectively [125], which would drop when the OPC content reduced. For instance, the mixture containing 50% OPC and 50% GGBS exhibited the same initial static yield stress as compared with that incorporating 80% OPC and 20% FA, the embodied carbon and embodied energy of which were found to be 19.39-32.32% lower. When OPC, FA and SF were combined as the binder, the embodied carbon and embodied energy can be significantly reduced [126]. The embodied carbon of 3DPG mixtures ranged from 107.48 to 133.75 kg CO2.eq/m^3 [15, 34], which was much lower than that of 3D printed cementitious materials. For instance, under a similar range of 28-d compressive strength, the 3DPG mixture (50%FA+50%GGBS) showed a 58.97% lower embodied carbon than 3D printed cementitious mixture (OPC41%+FA39%+SF20%). Regarding the embodied energy, the 3DPG mixtures had a higher value than the mixture containing FA, GGBS and SF but a lower value than the other two mixtures. As seen in Fig. 25, OPC, GGBS and superplasticiser had substantial contributions to the total embodied carbon and embodied energy of cementitious materials, while for 3DPG, the activator accounted for the biggest proportion of the total embodied carbon and embodied energy, which was confirmed by Yang et al. [136] that the embodied carbon of geopolymers was highly dependent on the type and dosage of the used activator.

The results above suggest that utilising 3DPG as a substitute for 3D printed cementitious materials can improve sustainability by mainly reducing carbon dioxide emissions, considering the phases before the concrete production. However, more phases (cradle-to-grave) as well as more printability-related properties (besides initial static yield stress) need to be considered for accurate assessment of sustainability of a specific type of structure.

Table 4. Life cycle inventory data of the ingredients collected from literature.

Material type	Embodied carbon (kg CO_2.eq/kg)	Embodied energy (MJ/kg)
OPC [127]	0.83	4.6
FA [127]	0.01	0.1
GGBS [127]	0.07	1.33
SF [128]	0.014	0.1
Sand [127]	0.005	0.1
Water	0	0
Superplasticiser [129, 130]	1.48	36.76
Sucrose [131]	0.307	0.822
Anhydrous Na_2SiO_3 [132]	0.93	17.9
NaOH pellet [124]	0.43	4.6
Na_2SiO_3 [132]	0.86	18

Table 5. Calculated embodied carbon and embodied energy.

Ref.	Binder	Embodied carbon (kg CO_2.eq/m^3)	Embodied energy (MJ/ m^3)	Initial static yield stress (Pa)	28-d compressive strength (MPa)
[125]	OPC80%+FA20%	555.51	3173.6	1600	-
[125]	OPC50%+GGBS50%	375.95	2558.13	1600	-
[126]	OPC41%+FA39%+SF20%	261.93	1754.72	13800	47.3-57.0
[15]	FA50%+GGBS50%	107.48	1933.31	870	44.7-61.2
[34]	FA78.5%+GGBS13.8%+SF7.7%	133.75	1930.92	800	-

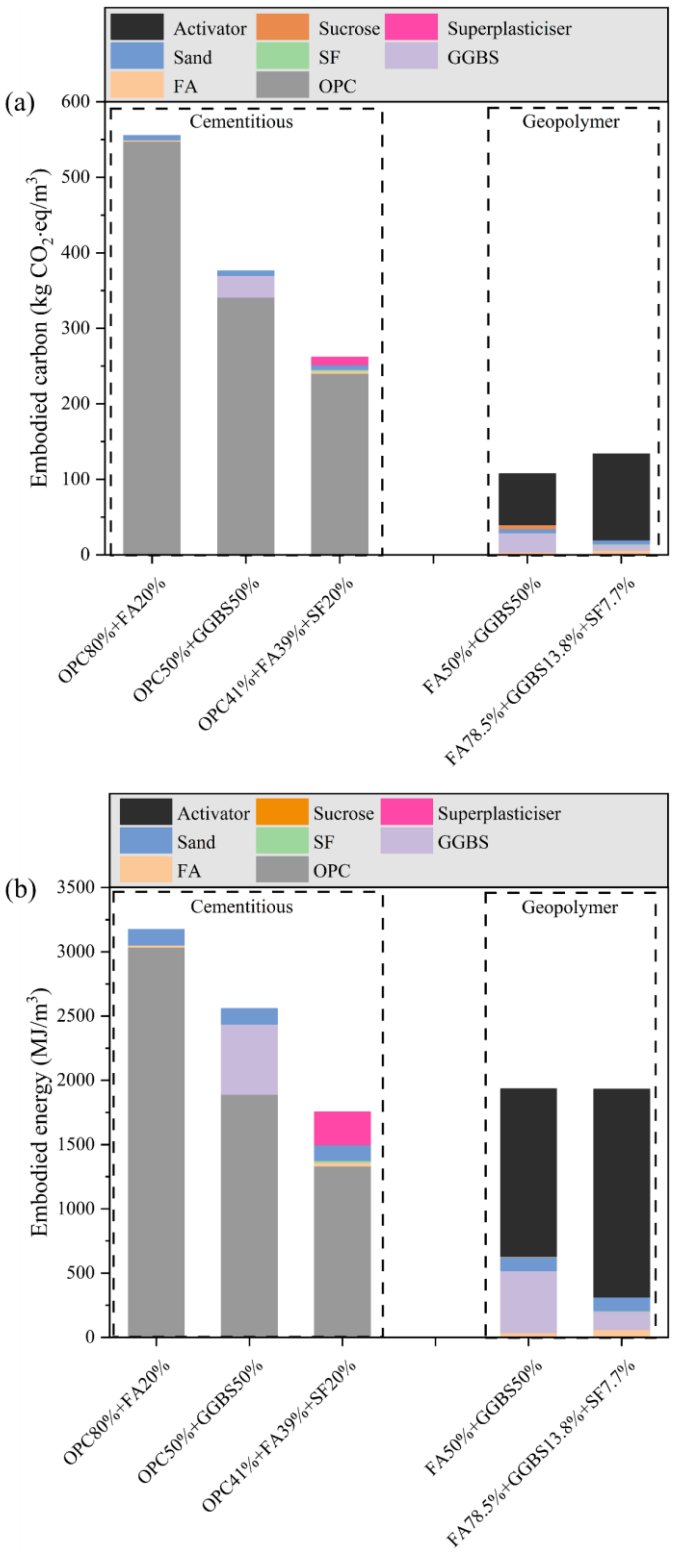

Fig. 25. Sustainability of 3D printed cementitious materials and 3DPG (based on **Table 2**).

6. Optimisation of mix design for 3D printed geopolymers

As mentioned in Section 1, the trial-and-error approach was adopted by the existing studies to determine the optimal mix design for 3DPG (Fig. 1). Table 6 lists a summary of potential optimal mix proportions of 3DPG, most of which were determined based on the fresh properties, especially one aspect of printability. For instance, Panda et al. [55] investigated the effects of two different additives (nano clay and hydromagnesite seed) on the fresh properties and microstructure of FA-

GGBS-SF based geopolymers and concluded that the mixture containing 0.4% nano clay and 2% hydromagnesite seed was the optimal one mainly considering the static yield stress, viscosity recovery ability, extrudability and buildability. As seen in Table 6, GGBS and SF were commonly used to replace FA at a replacement level of 5-50% and 2.5-15%, respectively. As discussed in Section 3.1, the presence of FA can provide high flowability and a long setting time for 3DPG, but lower buildability. Incorporating a certain amount of GGBS and SF can result in better buildability through increasing the rheological properties, including yield stress, viscosity, structural build-up and thixotropy. However, their contents should be carefully controlled as the extrudability and open time can be weakened if the incorporated dosages of them are too high. Both liquid and solid activators with different contents and moduli were used during the optimisation. Previous studies [15, 56] reported that the rapid dissolution of solid activator (e.g. anhydrous Na_2SiO_3) can lead to very high static yield stress after the mixing and its increase rate was also found to be significantly high. These can considerably reduce the pumpability, extrudability and particularly open time. To mitigate these issues, the content of the solid activator should be limited [53, 56] or replacing the anhydrous Na_2SiO_3 with another activator with a higher modulus [15] or utilising additives, e.g., sucrose [15, 56]. As a kind of retarder, the incorporation of sucrose can help limit the structural build-up of geopolymers, which can result in sufficient extrudability and open time. The content of used sucrose was either 0.5% or 1.5% if combined with other thixotropic additives. Other additives such as nano clay and hydromagnesite seed were also used to improve the printability of 3DPG. River sand with relatively small sizes was usually utilised as fine aggregates and its incorporated content was normally higher than that of binder (Agg/b: 1.5). It was reported that this content should be limited to ensure sufficient printability for 3DPG [34]. As indicated in Table 6, only one study [34] considered the incorporation of fibres during the optimisation of the mix design to improve the buildability of 3DPG. Depending on the mix design, production technique and curing regime, the compressive strength of 3DPG was in the range of 18.4-61.2 MPa. Most of the existing studies did not consider hardened properties, e.g., shrinkage, mechanical properties and durability for the optimisation of mix proportions, which are crucial for engineering applications. Regarding sustainability, the use of FA and GGBS as alternatives to OPC can reduce the carbon footprint, while the production of activators for 3DPG can emit a certain amount of carbon dioxide emissions (Fig. 25). For instance, Na_2SiO_3 was regarded as the highest contributor of carbon dioxide emissions compared to other raw materials for geopolymers [137, 138]. Moreover, the high alkalinity of NaOH solution can bring some handling issues during the production of geopolymers [139, 140]. Hence, to optimise the mix design for 3DPG, safer and more sustainable and cost-effective activators should be considered. Table 6 provides some general information on the potentially suitable mix proportions for developing 3DPG, while the ranges of them are still wide and rough due to the limited data available in the literature to date, which can be

further refined after more experimental data are obtained from future studies and included for practical applications.

7. Conclusions

Due to the demand for improving the sustainability of construction industry, geopolymers have been increasingly implemented in various applications, particularly in 3D printing construction lately. This paper comprehensively reviews recent advances in the development of extrusion-based 3D printed geopolymers (3DPG), mainly focusing on the matrix composition, reinforcement type, curing condition and printing configuration as well as their effects on fresh and hardened properties of 3DPG. The relationship between key fresh properties and printability related properties are well summarised and discussed.

Printable geopolymers should possess adequate printability including pumpability, extrudability, open time, buildability, and shape retention ability, which are governed by the fresh properties of geopolymers especially rheology. To achieve optimal printability, a balance between different types of fresh properties should be met, which can be tailored by altering the mix design of geopolymers mainly using the trial-and-error approach. Moreover, it is also essential to consider the mechanical properties and durability of 3DPG. Although utilising some additives (e.g., nano clay) can effectively improve the printability of geopolymers, the mechanical properties could be weakened when the threshold content of the incorporated additive is exceeded. Due to the unique process of 3D printing, the size of aggregate and the type of fibre are often limited, which may lower the shrinkage resistance and restrain the improvement of tensile properties for 3DPG. The hardened properties of 3DPG are related to the properties of the matrix and the bond behaviour between layers, which are governed by fresh properties of printed materials (e.g., structural build-up) and printing configurations (e.g., printing speed and printing layer cycle time). Besides, applying microwave heating after the deposition can enhance the bond strength of 3DPG, where this heating system implemented at the print-head can be considered as a potential set-on-demand method for geopolymers. The sustainability of 3D printed concrete can be significantly improved when geopolymer binders are used to replace Portland cement, considering mainly the carbon dioxide emissions. For instance, the use of fly ash and slag as the binder leads to a 58.97-80.65% reduction in embodied carbon as compared with some printable cementitious mixtures. For 3DPG, the potential optimal mixtures are suggested to contain a large amount of fly ash, a small amount of ground granulated blast-furnace slag and silica fume, liquid or solid activator (e.g., anhydrous Na_2SiO_3), river sand with size less than 2 mm, thixotropic additive (e.g., nano clay) and retarder (e.g., sucrose). Further experimental studies are required to enrich the data for optimising the mix proportions of 3DPG for practical engineering applications.

Although several types of 3DPG have been successfully developed, some remaining challenges need to be addressed for future research. It is important to study the effect of different mixing parameters such as adding sequence and mixing speed on the fresh and hardened properties of 3DPG, and thus a consistent mixing protocol can be developed when a similar mix design is implemented. The buildability of geopolymers is usually modified by adjusting the parameters in mix design, which is not so effective. To ensure the buildability requirements can be fulfilled accurately and timely after the extrusion, some set-on-demand methods are required. For better enhancing the mechanical properties while eliminating the anisotropic features for 3DPG, more studies should be conducted considering the effects of printing configuration, fibre reinforcement (e.g., hybrid fibres) and loading type (e.g., dynamic loading). It is necessary to consider the fresh properties of materials (especially structural build-up) for the optimisation of printing configuration and mitigation of anisotropic behaviour. To further promote the engineering applications, drying shrinkage, and durability of 3DPG need to be investigated. The sustainability assessment of 3DPG in the cradle-to-grave phase is required, including more relevant functional indicators (e.g., buildability) in the analysis. Each aspect of printability and some key hardened properties should be considered for the optimisation of mix proportions for 3DPG, selecting safer and more eco-friendly activators and certain reinforcements.

Acknowledgements

The authors gratefully acknowledge the financial support from the Engineering and Physical Sciences Research Council (EPSRC), UK under Grant No. EP/R041504/1 and the Royal Society, UK under Award No. IEC\NSFC\191417 as well as the Visiting Researcher Fund Program of State Key Laboratory of Water Resources and Hydropower Engineering Science, China under Award No. 2019SGG01. The financial support provided by University College London (UCL) and China Scholarship Council (CSC) to the first author is gratefully acknowledged.

Table 6. Summary of potential optimal mix proportions for 3DPG.

Ref.	Binder	Activator	L/b (or W/s)	Aggregate (Agg/b)	Additive (Add/b)	Fibre (volume, %)	Curing condition	Compressive strength
[14]	FA:GGBS:SF (0.9:0.05:0.05)	NaOH+Na_2SiO_3	L/b (0.46)	River sand (1.5)	-	-	Ambient temperature (25 ± 2 °C)	7 d: 18.4 MPa
[34]	FA:GGBS:SF (0.785:0.138:0.077)	NaOH+Na_2SiO_3	L/b (0.49)	River sand (1.5)	Nano clay (0.012)	Glass fibre (0.25)	-	-
[53]	FA:GGBS (0.7:0.3)	KOH+K_2SiO_3	W/s (0.35)	River sand (0.85)	-	-	Ambient temperature	28 d: 24.4-28.3 MPa
[54]	FA:GGBS:SF (0.775:0.2:0.025)	Na_2SO_4	-	River sand (1.35)	-	-	-	-
[36]	FA:GGBS:SF (0.6:0.25:0.15)	NaOH+Na_2SiO_3	L/b (0.18)	River sand (0.55)	-	-	60 °C for 24 h, then ambient temperature (20 °C)	7 d: 43.9-50.1 MPa
[37]	FA:GGBS:SF (0.8:0.1:0.1)	Anhydrous Na_2SiO_3	W/s (0.27)	Quartz sand (1.5)	Thixotropic additive (0.01)	-	-	-
[55]	GGBS (1.0)	$Na_2SiO_3·5H_2O$	-	Sand (0.83)	Nano clay (0.004)+Hydromagnesite seed (0.02)	-	-	-
[15]	FA:GGBS (0.5:0.5)	GD grade Na_2SiO_3+Anhydrous Na_2SiO_3	W/s (0.34)	Sand (1.5)	Sucrose (0.005)	-	60 °C for 24 h, then ambient temperature, Ambient temperature (23 ± 3 °C)	28 d: 44.7-61.2 MPa
[56]	FA:GGBS (0.5:0.5)	Anhydrous Na_2SiO_3	W/s (0.327)	Sand (1.5)	Sucrose (0.015)+ Highly purified Magnesium Alumino Silicate (0.0075)	-	Water	7 d: 22-35 MPa 28 d: 35.8-45.0 MPa

Note: Add/b: Additive-to-binder ratio.

References

[1] T. Wangler, N. Roussel, F.P. Bos, T.A.M. Salet, R.J. Flatt, Digital Concrete: A Review, Cement and Concrete Research 123 (2019) 105780.

[2] M.K. Mohan, A.V. Rahul, G. De Schutter, K. Van Tittelboom, Extrusion-based concrete 3D printing from a material perspective: A state-of-the-art review, Cement and Concrete Composites 115 (2021) 103855.

[3] T.D. Ngo, A. Kashani, G. Imbalzano, K.T.Q. Nguyen, D. Hui, Additive manufacturing (3D printing): A review of materials, methods, applications and challenges, Composites Part B: Engineering 143 (2018) 172-196.

[4] J. Zhang, J. Wang, S. Dong, X. Yu, B. Han, A review of the current progress and application of 3D printed concrete, Composites Part A: Applied Science and Manufacturing 125 (2019) 105533.

[5] M.S. Khan, F. Sanchez, H. Zhou, 3-D printing of concrete: Beyond horizons, Cement and Concrete Research 133 (2020) 106070.

[6] B. Khoshnevis, D. Hwang, K.-T. Yao, Z.J.I.J.o.I. Yeh, S. Engineering, Mega-scale fabrication by contour crafting, 1(3) (2006) 301-320.

[7] G. Cesaretti, E. Dini, X. De Kestelier, V. Colla, L. Pambaguian, Building components for an outpost on the Lunar soil by means of a novel 3D printing technology, Acta Astronaut. 93 (2014) 430-450.

[8] R.A. Buswell, W.R. Leal de Silva, S.Z. Jones, J. Dirrenberger, 3D printing using concrete extrusion: A roadmap for research, Cement and Concrete Research 112 (2018) 37-49.

[9] C. Zhang, V.N. Nerella, A. Krishna, S. Wang, Y. Zhang, V. Mechtcherine, N. Banthia, Mix design concepts for 3D printable concrete: A review, Cement and Concrete Composites 122 (2021) 104155.

[10] M.K. Mohan, A.V. Rahul, K. Van Tittelboom, G. De Schutter, Rheological and pumping behaviour of 3D printable cementitious materials with varying aggregate content, Cement and Concrete Research 139 (2021) 106258.

[11] Z. Zhang, F. Yang, J.-C. Liu, S. Wang, Eco-friendly high strength, high ductility engineered cementitious composites (ECC) with substitution of fly ash by rice husk ash, Cement and Concrete Research 137 (2020) 106200.

[12] T. Luukkonen, Z. Abdollahnejad, J. Yliniemi, P. Kinnunen, M. Illikainen, One-part alkali-activated materials: A review, Cement and Concrete Research 103 (2018) 21-34.

[13] B. Panda, S.C. Paul, L.J. Hui, Y.W.D. Tay, M.J. Tan, Additive manufacturing of geopolymer for sustainable built environment, Journal of Cleaner Production 167 (2017) 281-288.

[14] B. Panda, C. Unluer, M.J. Tan, Investigation of the rheology and strength of geopolymer mixtures for extrusion-based 3D printing, Cement and Concrete Composites 94 (2018) 307-314.

[15] S.H. Bong, M. Xia, B. Nematollahi, C. Shi, Ambient temperature cured 'just-add-water' geopolymer for 3D concrete printing applications, Cement and Concrete Composites 121 (2021).
[16] M. Xia, J.G. Sanjayan, Methods of enhancing strength of geopolymer produced from powder-based 3D printing process, Materials Letters 227 (2018) 281-283.
[17] V. Voney, P. Odaglia, C. Brumaud, B. Dillenburger, G. Habert, From casting to 3D printing geopolymers: A proof of concept, Cement and Concrete Research 143 (2021).
[18] N. Ranjbar, C. Kuenzel, J. Spangenberg, M. Mehrali, Hardening evolution of geopolymers from setting to equilibrium: A review, Cement and Concrete Composites 114 (2020) 103729.
[19] N. Roussel, Rheological requirements for printable concretes, Cement and Concrete Research 112 (2018) 76-85.
[20] B. Lu, Y. Weng, M. Li, Y. Qian, K.F. Leong, M.J. Tan, S. Qian, A systematical review of 3D printable cementitious materials, Construction and Building Materials 207 (2019) 477-490.
[21] S. Bhattacherjee, A.S. Basavaraj, A.V. Rahul, M. Santhanam, R. Gettu, B. Panda, E. Schlangen, Y. Chen, O. Copuroglu, G. Ma, L. Wang, M.A. Basit Beigh, V. Mechtcherine, Sustainable materials for 3D concrete printing, Cement and Concrete Composites 122 (2021) 104156.
[22] M. Xia, J. Sanjayan, Method of formulating geopolymer for 3D printing for construction applications, Materials & Design 110 (2016) 382-390.
[23] B. Nematollahi, M. Xia, J. Sanjayan, Post-processing Methods to Improve Strength of Particle-Bed 3D Printed Geopolymer for Digital Construction Applications, Frontiers in Materials 6 (2019).
[24] Z. Zuhua, Y. Xiao, Z. Huajun, C. Yue, Role of water in the synthesis of calcined kaolin-based geopolymer, Applied Clay Science 43(2) (2009) 218-223.
[25] H. Wang, H. Li, F. Yan, Synthesis and mechanical properties of metakaolinite-based geopolymer, Colloids and Surfaces A: Physicochemical and Engineering Aspects 268(1) (2005) 1-6.
[26] L. Weng, K.J.J.o.m.s. Sagoe-Crentsil, Dissolution processes, hydrolysis and condensation reactions during geopolymer synthesis: Part I—Low Si/Al ratio systems, 42(9) (2007) 2997-3006.
[27] N. Ranjbar, M. Mehrali, C. Kuenzel, C. Gundlach, D.B. Pedersen, A. Dolatshahi-Pirouz, J. Spangenberg, Rheological characterization of 3D printable geopolymers, Cement and Concrete Research 147 (2021).
[28] T. Antonić, A. Čizmek, C. Kosanović, B. Subotić, Dissolution of amorphous aluminosilicate zeolite precursors in alkaline solutions. Part 1.—Kinetics of the dissolution, Journal of the Chemical Society, Faraday Transactions 89(11) (1993) 1817-1822.
[29] U. Rattanasak, P. Chindaprasirt, Influence of NaOH solution on the synthesis of fly ash geopolymer, Miner. Eng. 22(12) (2009) 1073-1078.

[30] J. Davidovits, Properties of geopolymer cements, First international conference on alkaline cements and concretes, Kiev State Technical University, Ukraine: Scientific Research Institute on …, 1994, pp. 131-149.
[31] A. Hajimohammadi, J.L. Provis, J.S.J.C.o.M. Van Deventer, Effect of alumina release rate on the mechanism of geopolymer gel formation, 22(18) (2010) 5199-5208.
[32] G. Görhan, G. Kürklü, The influence of the NaOH solution on the properties of the fly ash-based geopolymer mortar cured at different temperatures, Composites Part B: Engineering 58 (2014) 371-377.
[33] E.N. Kani, A.J.J.o.M.s. Allahverdi, Effects of curing time and temperature on strength development of inorganic polymeric binder based on natural pozzolan, Journal of Materials Science 44(12) (2009) 3088-3097.
[34] B. Panda, M.J. Tan, Experimental study on mix proportion and fresh properties of fly ash based geopolymer for 3D concrete printing, Ceramics International 44(9) (2018) 10258-10265.
[35] B. Panda, S.C. Paul, N.A.N. Mohamed, Y.W.D. Tay, M.J. Tan, Measurement of tensile bond strength of 3D printed geopolymer mortar, Measurement 113 (2018) 108-116.
[36] M. Chougan, S. Hamidreza Ghaffar, M. Jahanzat, A. Albar, N. Mujaddedi, R. Swash, The influence of nano-additives in strengthening mechanical performance of 3D printed multi-binder geopolymer composites, Construction and Building Materials 250 (2020) 118928.
[37] X. Guo, J. Yang, G. Xiong, Influence of supplementary cementitious materials on rheological properties of 3D printed fly ash based geopolymer, Cement and Concrete Composites 114 (2020) 103820.
[38] B. Panda, N.A. Noor Mohamed, Y.W.D. Tay, M.J. Tan, Bond Strength in 3D Printed Geopolymer Mortar, in: T. Wangler, R.J. Flatt (Eds.) First RILEM International Conference on Concrete and Digital Fabrication – Digital Concrete 2018, Springer International Publishing, Cham, 2019, pp. 200-206.
[39] J.H. Lim, B. Panda, Q.-C. Pham, Improving flexural characteristics of 3D printed geopolymer composites with in-process steel cable reinforcement, Construction and Building Materials 178 (2018) 32-41.
[40] B. Panda, S. Chandra Paul, M. Jen Tan, Anisotropic mechanical performance of 3D printed fiber reinforced sustainable construction material, Materials Letters 209 (2017) 146-149.
[41] G. Ma, Z. Li, L. Wang, G. Bai, Micro-cable reinforced geopolymer composite for extrusion-based 3D printing, Materials Letters 235 (2019) 144-147.
[42] Z. Li, L. Wang, G. Ma, Mechanical improvement of continuous steel microcable reinforced geopolymer composites for 3D printing subjected to different loading conditions, Composites Part B: Engineering 187 (2020) 107796.

[43] H. Alghamdi, S.A.O. Nair, N. Neithalath, Insights into material design, extrusion rheology, and properties of 3D-printable alkali-activated fly ash-based binders, Materials & Design 167 (2019) 107634.
[44] M. Tramontin Souza, L. Simão, E. Guzi de Moraes, L. Senff, J.R. de Castro Pessôa, M.J. Ribeiro, A.P. Novaes de Oliveira, Role of temperature in 3D printed geopolymers: Evaluating rheology and buildability, Materials Letters 293 (2021).
[45] D.-W. Zhang, D.-m. Wang, X.-Q. Lin, T. Zhang, The study of the structure rebuilding and yield stress of 3D printing geopolymer pastes, Construction and Building Materials 184 (2018) 575-580.
[46] C. Sun, J. Xiang, M. Xu, Y. He, Z. Tong, X. Cui, 3D extrusion free forming of geopolymer composites: Materials modification and processing optimization, Journal of Cleaner Production 258 (2020).
[47] S. Al-Qutaifi, A. Nazari, A. Bagheri, Mechanical properties of layered geopolymer structures applicable in concrete 3D-printing, Construction and Building Materials 176 (2018) 690-699.
[48] V. Mechtcherine, V.N. Nerella, F. Will, M. Näther, J. Otto, M. Krause, Large-scale digital concrete construction – CONPrint3D concept for on-site, monolithic 3D-printing, Automation in Construction 107 (2019) 102933.
[49] S. Kawashima, K. Wang, R.D. Ferron, J.H. Kim, N. Tregger, S. Shah, A review of the effect of nanoclays on the fresh and hardened properties of cement-based materials, Cement and Concrete Research 147 (2021) 106502.
[50] S. Muthukrishnan, S. Ramakrishnan, J. Sanjayan, Effect of microwave heating on interlayer bonding and buildability of geopolymer 3D concrete printing, Construction and Building Materials 265 (2020).
[51] S.H. Bong, B. Nematollahi, M. Xia, A. Nazari, J. Sanjayan, J. Pan, Properties of 3D-Printable Ductile Fibre-Reinforced Geopolymer Composite for Digital Construction Applications, in: V. Mechtcherine, K. Khayat, E. Secrieru (Eds.) Rheology and Processing of Construction Materials, Springer International Publishing, Cham, 2020, pp. 363-372.
[52] B. Panda, C. Unluer, M.J. Tan, Extrusion and rheology characterization of geopolymer nanocomposites used in 3D printing, Composites Part B: Engineering 176 (2019) 107290.
[53] B. Panda, G.V.P.B. Singh, C. Unluer, M.J. Tan, Synthesis and characterization of one-part geopolymers for extrusion based 3D concrete printing, Journal of Cleaner Production 220 (2019) 610-619.
[54] B. Panda, M.J. Tan, Rheological behavior of high volume fly ash mixtures containing micro silica for digital construction application, Materials Letters 237 (2019) 348-351.

[55] B. Panda, S. Ruan, C. Unluer, M.J. Tan, Investigation of the properties of alkali-activated slag mixes involving the use of nanoclay and nucleation seeds for 3D printing, Composites Part B: Engineering 186 (2020).
[56] S. Muthukrishnan, S. Ramakrishnan, J. Sanjayan, Effect of alkali reactions on the rheology of one-part 3D printable geopolymer concrete, Cement and Concrete Composites 116 (2021).
[57] S.H. Bong, B. Nematollahi, A. Nazari, M. Xia, J.G. Sanjayan, Fresh and Hardened Properties of 3D Printable Geopolymer Cured in Ambient Temperature, in: T. Wangler, R.J. Flatt (Eds.) First RILEM International Conference on Concrete and Digital Fabrication – Digital Concrete 2018, Springer International Publishing, Cham, 2019, pp. 3-11.
[58] B. Nematollahi, M. Xia, S.H. Bong, J. Sanjayan, Hardened Properties of 3D Printable 'One-Part' Geopolymer for Construction Applications, in: T. Wangler, R.J. Flatt (Eds.) First RILEM International Conference on Concrete and Digital Fabrication – Digital Concrete 2018, Springer International Publishing, Cham, 2019, pp. 190-199.
[59] V. Mechtcherine, F.P. Bos, A. Perrot, W.R.L. da Silva, V.N. Nerella, S. Fataei, R.J.M. Wolfs, M. Sonebi, N. Roussel, Extrusion-based additive manufacturing with cement-based materials – Production steps, processes, and their underlying physics: A review, Cement and Concrete Research 132 (2020) 106037.
[60] V.C. Li, F.P. Bos, K. Yu, W. McGee, T.Y. Ng, S.C. Figueiredo, K. Nefs, V. Mechtcherine, V.N. Nerella, J. Pan, G.P.A.G. van Zijl, P.J. Kruger, On the emergence of 3D printable Engineered, Strain Hardening Cementitious Composites (ECC/SHCC), Cement and Concrete Research 132 (2020) 106038.
[61] G. Ma, Z. Li, L. Wang, F. Wang, J. Sanjayan, Mechanical anisotropy of aligned fiber reinforced composite for extrusion-based 3D printing, Construction and Building Materials 202 (2019) 770-783.
[62] Y. Alrefaei, Y.-S. Wang, J.-G. Dai, Effect of mixing method on the performance of alkali-activated fly ash/slag pastes along with polycarboxylate admixture, Cement and Concrete Composites 117 (2021) 103917.
[63] N. Ranjbar, M. Zhang, Fiber-reinforced geopolymer composites: A review, Cement and Concrete Composites 107 (2020) 103498.
[64] A.H. Mahmood, S.J. Foster, A. Castel, Effects of mixing duration on engineering properties of geopolymer concrete, Construction and Building Materials 303 (2021) 124449.
[65] M. Palacios, F. Puertas, Effectiveness of mixing time on hardened properties of waterglass-activated slag pastes and mortars, ACI Mater. J. 108(1) (2011) 73.
[66] F. Puertas, B. González-Fonteboa, I. González-Taboada, M.M. Alonso, M. Torres-Carrasco, G. Rojo, F. Martínez-Abella, Alkali-activated slag concrete: Fresh and hardened behaviour, Cement and Concrete Composites 85 (2018) 22-31.

[67] J. Xiao, G. Ji, Y. Zhang, G. Ma, V. Mechtcherine, J. Pan, L. Wang, T. Ding, Z. Duan, S. Du, Large-scale 3D printing concrete technology: Current status and future opportunities, Cement and Concrete Composites 122 (2021) 104115.
[68] C. Gosselin, R. Duballet, P. Roux, N. Gaudillière, J. Dirrenberger, P. Morel, Large-scale 3D printing of ultra-high performance concrete – a new processing route for architects and builders, Materials & Design 100 (2016) 102-109.
[69] F. Bos, R. Wolfs, Z. Ahmed, T. Salet, Additive manufacturing of concrete in construction: potentials and challenges of 3D concrete printing, Virtual and Physical Prototyping 11(3) (2016) 209-225.
[70] A.S.J. Suiker, R.J.M. Wolfs, S.M. Lucas, T.A.M. Salet, Elastic buckling and plastic collapse during 3D concrete printing, Cement and Concrete Research 135 (2020) 106016.
[71] S. Muthukrishnan, S. Ramakrishnan, J. Sanjayan, Technologies for improving buildability in 3D concrete printing, Cement and Concrete Composites 122 (2021) 104144.
[72] R.J.M. Wolfs, A.S.J. Suiker, Structural failure during extrusion-based 3D printing processes, The International Journal of Advanced Manufacturing Technology 104(1) (2019) 565-584.
[73] T.T. Le, S.A. Austin, S. Lim, R.A. Buswell, A.G.F. Gibb, T. Thorpe, Mix design and fresh properties for high-performance printing concrete, Materials and Structures 45(8) (2012) 1221-1232.
[74] M. Choi, N. Roussel, Y. Kim, J. Kim, Lubrication layer properties during concrete pumping, Cement and Concrete Research 45 (2013) 69-78.
[75] R.P. Chhabra, J.F. Richardson, in: R.P. Chhabra, J.F. Richardson (Eds.), Non-Newtonian Flow and Applied Rheology (Second Edition), Butterworth-Heinemann, Oxford, 2008, pp. 1-55.
[76] S.-D. Jo, C.-K. Park, J.-H. Jeong, S.-H. Lee, S.-H. Kwon, A Computational Approach to Estimating a Lubricating Layer in Concrete Pumping, 27(3) (2012) 189--210.
[77] S. Lim, R.A. Buswell, T.T. Le, S.A. Austin, A.G.F. Gibb, T. Thorpe, Developments in construction-scale additive manufacturing processes, Automation in Construction 21 (2012) 262-268.
[78] W. Timothy, L. Ena, R. Lex, H. Norman, G. Fabio, K. Matthias, B. Mathias, D. Benjamin, B. Jonas, R. Nicolas, F. Robert, Digital Concrete: Opportunities and Challenges, RILEM Technical Letters 1(0) (2016).
[79] N. Roussel, G. Ovarlez, S. Garrault, C. Brumaud, The origins of thixotropy of fresh cement pastes, Cement and Concrete Research 42(1) (2012) 148-157.
[80] D. Marchon, S. Kawashima, H. Bessaies-Bey, S. Mantellato, S. Ng, Hydration and rheology control of concrete for digital fabrication: Potential admixtures and cement chemistry, Cement and Concrete Research 112 (2018) 96-110.
[81] G. Ovarlez, N. Roussel, A Physical Model for the Prediction of Lateral Stress Exerted by Self-Compacting Concrete on Formwork, Materials and Structures 39(2) (2006) 269-279.

[82] A. Aboulayt, M. Riahi, M. Ouazzani Touhami, H. Hannache, M. Gomina, R. Moussa, Properties of metakaolin based geopolymer incorporating calcium carbonate, Adv. Powder Technol. 28(9) (2017) 2393-2401.
[83] J. Shang, J.-G. Dai, T.-J. Zhao, S.-Y. Guo, P. Zhang, B. Mu, Alternation of traditional cement mortars using fly ash-based geopolymer mortars modified by slag, Journal of Cleaner Production 203 (2018) 746-756.
[84] P.S. Deb, P. Nath, P.K. Sarker, The effects of ground granulated blast-furnace slag blending with fly ash and activator content on the workability and strength properties of geopolymer concrete cured at ambient temperature, Materials & Design (1980-2015) 62 (2014) 32-39.
[85] C. Lu, Z. Zhang, C. Shi, N. Li, D. Jiao, Q. Yuan, Rheology of alkali-activated materials: A review, Cement and Concrete Composites 121 (2021) 104061.
[86] T. Yang, H. Zhu, Z. Zhang, X. Gao, C. Zhang, Q. Wu, Effect of fly ash microsphere on the rheology and microstructure of alkali-activated fly ash/slag pastes, Cement and Concrete Research 109 (2018) 198-207.
[87] H. Güllü, A. Cevik, K.M.A. Al-Ezzi, M.E. Gülsan, On the rheology of using geopolymer for grouting: A comparative study with cement-based grout included fly ash and cold bonded fly ash, Construction and Building Materials 196 (2019) 594-610.
[88] S. Grünewald, 9 - Fibre reinforcement and the rheology of concrete, in: N. Roussel (Ed.), Understanding the Rheology of Concrete, Woodhead Publishing2012, pp. 229-256.
[89] H. Zhong, M. Zhang, Experimental study on engineering properties of concrete reinforced with hybrid recycled tyre steel and polypropylene fibres, Journal of Cleaner Production 259 (2020) 120914.
[90] D. Hardjito, M. Tsen, Strength and thermal stability of fly ash-based geopolymer mortar, The 3rd International Conference-ACF/VCA, 2008, pp. 144-150.
[91] N.K. Lee, H.K. Lee, Setting and mechanical properties of alkali-activated fly ash/slag concrete manufactured at room temperature, Construction and Building Materials 47 (2013) 1201-1209.
[92] I. Ismail, S.A. Bernal, J.L. Provis, R. San Nicolas, S. Hamdan, J.S.J. van Deventer, Modification of phase evolution in alkali-activated blast furnace slag by the incorporation of fly ash, Cement and Concrete Composites 45 (2014) 125-135.
[93] D. Jiao, R. De Schryver, C. Shi, G. De Schutter, Thixotropic structural build-up of cement-based materials: A state-of-the-art review, Cement and Concrete Composites 122 (2021) 104152.
[94] N. Roussel, A thixotropy model for fresh fluid concretes: Theory, validation and applications, Cement and Concrete Research 36(10) (2006) 1797-1806.
[95] D. Feys, R. Cepuritis, S. Jacobsen, K. Lesage, E. Secrieru, A. Yahia, Measuring rheological properties of cement pastes: most common techniques, procedures and challenges, RILEM Technical Letters 2 (2018) 129-135.

[96] J. Xiang, L. Liu, X. Cui, Y. He, G. Zheng, C. Shi, Effect of limestone on rheological, shrinkage and mechanical properties of alkali – Activated slag/fly ash grouting materials, Construction and Building Materials 191 (2018) 1285-1292.
[97] D. Rieger, J. Kadlec, M. Pola, T. Kovářík, P. Franče, Mechanical properties of non-woven glass fiber geopolymer composites, IOP Conference Series: Materials Science and Engineering 175 (2017) 012054.
[98] G. Fang, W.K. Ho, W. Tu, M. Zhang, Workability and mechanical properties of alkali-activated fly ash-slag concrete cured at ambient temperature, Construction and Building Materials 172 (2018) 476-487.
[99] B. Sun, Y. Sun, G. Ye, G. De Schutter, A mix design methodology of slag and fly ash-based alkali-activated paste, Cement and Concrete Composites 126 (2022) 104368.
[100] A. Zingg, F. Winnefeld, L. Holzer, J. Pakusch, S. Becker, L. Gauckler, Adsorption of polyelectrolytes and its influence on the rheology, zeta potential, and microstructure of various cement and hydrate phases, J. Colloid Interface Sci. 323(2) (2008) 301-312.
[101] S.H. Chang, M.H. Ryan, R.K. Gupta, The effect of pH, ionic strength, and temperature on the rheology and stability of aqueous clay suspensions, Rheol. Acta 32(3) (1993) 263-269.
[102] P. Coussot, 1 - Introduction to the rheology of complex fluids, in: N. Roussel (Ed.), Understanding the Rheology of Concrete, Woodhead Publishing2012, pp. 3-22.
[103] C.F. Ferraris, N.S. Martys, 3 - Concrete rheometers, in: N. Roussel (Ed.), Understanding the Rheology of Concrete, Woodhead Publishing2012, pp. 63-82.
[104] K. Vance, A. Dakhane, G. Sant, N. Neithalath, Observations on the rheological response of alkali activated fly ash suspensions: the role of activator type and concentration, Rheol. Acta 53(10) (2014) 843-855.
[105] V. Glukhovskij, Y. Zaitsev, V. Pakhomov, Slag-alkaline cements and concretes-structure, properties, technological and economical aspects of the use, J Silicates industriels 48(10) (1983) 197-200.
[106] M.F. Alnahhal, T. Kim, A. Hajimohammadi, Distinctive rheological and temporal viscoelastic behaviour of alkali-activated fly ash/slag pastes: A comparative study with cement paste, Cement and Concrete Research 144 (2021).
[107] B. Panda, S. Ruan, C. Unluer, M.J. Tan, Improving the 3D printability of high volume fly ash mixtures via the use of nano attapulgite clay, Composites Part B: Engineering 165 (2019) 75-83.
[108] S. Ma, Y. Qian, S. Kawashima, Experimental and modeling study on the non-linear structural build-up of fresh cement pastes incorporating viscosity modifying admixtures, Cement and Concrete Research 108 (2018) 1-9.

[109] D. Feys, A. Asghari, Influence of maximum applied shear rate on the measured rheological properties of flowable cement pastes, Cement and Concrete Research 117 (2019) 69-81.
[110] L.R. Prudêncio, Accelerating admixtures for shotcrete, Cement and Concrete Composites 20(2) (1998) 213-219.
[111] L. Reiter, T. Wangler, A. Anton, R.J. Flatt, Setting on demand for digital concrete – Principles, measurements, chemistry, validation, Cement and Concrete Research 132 (2020) 106047.
[112] J.L. Provis, S.A. Bernal, Geopolymers and Related Alkali-Activated Materials, 44(1) (2014) 299-327.
[113] P. Duxson, A. Fernández-Jiménez, J.L. Provis, G.C. Lukey, A. Palomo, J.S.J. van Deventer, Geopolymer technology: the current state of the art, Journal of Materials Science 42(9) (2007) 2917-2933.
[114] H. Freundlich, F. Juliusburger, Thixotropy, influenced by the orientation of anisometric particles in sols and suspensions, Transactions of the Faraday Society 31(0) (1935) 920-921.
[115] J. Mewis, N.J. Wagner, Thixotropy, Adv. Colloid Interface Sci. 147-148 (2009) 214-227.
[116] G. Ma, J. Zhang, L. Wang, Z. Li, J. Sun, Mechanical characterization of 3D printed anisotropic cementitious material by the electromechanical transducer, Smart Materials and Structures 27(7) (2018) 075036.
[117] N.K. Lee, J.G. Jang, H.K. Lee, Shrinkage characteristics of alkali-activated fly ash/slag paste and mortar at early ages, Cement and Concrete Composites 53 (2014) 239-248.
[118] N. Ranjbar, M. Mehrali, M. Mehrali, U.J. Alengaram, M.Z. Jumaat, Graphene nanoplatelet-fly ash based geopolymer composites, Cement and Concrete Research 76 (2015) 222-231.
[119] J. Yu, J. Yao, X. Lin, H. Li, J.Y.K. Lam, C.K.Y. Leung, I.M.L. Sham, K. Shih, Tensile performance of sustainable Strain-Hardening Cementitious Composites with hybrid PVA and recycled PET fibers, Cement and Concrete Research 107 (2018) 110-123.
[120] N. Ranjbar, M. Zhang, Fiber reinforced geopolymer composites: A review, Cement and Concrete Composites (2019) 103498.
[121] B. Zhu, J. Pan, B. Nematollahi, Z. Zhou, Y. Zhang, J. Sanjayan, Development of 3D printable engineered cementitious composites with ultra-high tensile ductility for digital construction, Materials & Design 181 (2019) 108088.
[122] K. Yu, W. McGee, T.Y. Ng, H. Zhu, V.C. Li, 3D-printable engineered cementitious composites (3DP-ECC): Fresh and hardened properties, Cement and Concrete Research 143 (2021).
[123] J. Ye, C. Cui, J. Yu, K. Yu, J. Xiao, Fresh and anisotropic-mechanical properties of 3D printable ultra-high ductile concrete with crumb rubber, Composites Part B: Engineering 211 (2021).
[124] M. Ohno, V.C. Li, An integrated design method of Engineered Geopolymer Composite, Cement and Concrete Composites 88 (2018) 73-85.

[125] A.V. Rahul, A. Sharma, M. Santhanam, A desorptivity-based approach for the assessment of phase separation during extrusion of cementitious materials, Cement and Concrete Composites 108 (2020) 103546.
[126] S.C. Paul, Y.W.D. Tay, B. Panda, M.J. Tan, Fresh and hardened properties of 3D printable cementitious materials for building and construction, Archives of Civil and Mechanical Engineering 18(1) (2018) 311-319.
[127] G. Hammond, C. Jones, F. Lowrie, P. Tse, Inventory of carbon & energy: ICE, Sustainable Energy Research Team, Department of Mechanical Engineering 2008.
[128] R. Sharma, R.A. Khan, Sustainable use of copper slag in self compacting concrete containing supplementary cementitious materials, Journal of Cleaner Production 151 (2017) 179-192.
[129] E.-H. Yang, Y. Yang, V.C. Li, Use of high volumes of fly ash to improve ECC mechanical properties and material greenness, ACI Mater. J. 104(6) (2007) 620-628.
[130] X. Huang, R. Ranade, V.C. Li, Feasibility study of developing green ECC using iron ore tailings powder as cement replacement, ACI Mater. J. 25(7) (2013) 923-931.
[131] P. Rein, The carbon footprint of sugar, Proc. Int. Soc. Sugar Cane Technol, 2010, p. 15.
[132] M. Fawer, M. Concannon, W. Rieber, Life cycle inventories for the production of sodium silicates, The International Journal of Life Cycle Assessment 4(4) (1999) 207.
[133] R. Gettu, R.G. Pillai, M. Santhanam, A.S. Basavaraj, S. Rathnarajan, B.S. Dhanya, Sustainability-based decision support framework for choosing concrete mixture proportions, Materials and Structures 51(6) (2018) 165.
[134] B.L. Damineli, F.M. Kemeid, P.S. Aguiar, V.M. John, Measuring the eco-efficiency of cement use, Cement and Concrete Composites 32(8) (2010) 555-562.
[135] R. Muigai, M. Alexander, P. Moyo, A novel framework towards the design of more sustainable concrete infrastructure, Materials and structures 49(4) (2016) 1127-1141.
[136] K.-H. Yang, J.-K. Song, K.-I. Song, Assessment of CO2 reduction of alkali-activated concrete, Journal of Cleaner Production 39 (2013) 265-272.
[137] A. Passuello, E.D. Rodríguez, E. Hirt, M. Longhi, S.A. Bernal, J.L. Provis, A.P. Kirchheim, Evaluation of the potential improvement in the environmental footprint of geopolymers using waste-derived activators, Journal of Cleaner Production 166 (2017) 680-689.
[138] X. Dai, S. Aydın, M.Y. Yardımcı, K. Lesage, G. De Schutter, Rheology and microstructure of alkali-activated slag cements produced with silica fume activator, Cement and Concrete Composites 125 (2022).
[139] Z. Zhang, J.L. Provis, A. Reid, H. Wang, Fly ash-based geopolymers: The relationship between composition, pore structure and efflorescence, Cement and Concrete Research 64 (2014) 30-41.

[140] X. Xue, Y.-L. Liu, J.-G. Dai, C.-S. Poon, W.-D. Zhang, P. Zhang, Inhibiting efflorescence formation on fly ash–based geopolymer via silane surface modification, Cement and Concrete Composites 94 (2018) 43-52.